ANL--92/38

DE93 007785

ANL-92/38

ARGONNE NATIONAL LABORATORY
9700 South Cass Avenue
Argonne, Illinois 60439

PRACTICAL SUPERCONDUCTOR DEVELOPMENT FOR ELECTRICAL POWER APPLICATIONS

ANNUAL REPORT FOR FY 1992

Roger B. Poeppel, Coordinator
Kenneth C. Goretta, Compiler

Contributors:

U. Balachandran
I. Bloom**
Y. S. Cha
N. Chen*
S. E. Dorris
E. D. Doss†
J. T. Dusek
J. E. Emerson
K. C. Goretta
K. E. Gray*
M. C. Hash**
J. D. Hettinger*
J. R. Hull
R. T. Kampwirth*
M. A. Kirk*
D. S. Kupperman
M. T. Lanagan
V. A. Maroni**
R. L. McDaniel
D. J. Miller*
R. C. Niemann
J. J. Picciolo
J. L. Routbort
J. P. Singh
K. L. Uherka
R. Wheeler*
C. A. Youngdahl

Materials and Components Technology Division

October 1992

Work supported by

U.S. DEPARTMENT OF ENERGY
Office of Energy Storage and Distribution

*Materials Science Division.
**Chemical Technology Division.
†Engineering Physics Division.

Contents

Figures

Tables

PRACTICAL SUPERCONDUCTOR DEVELOPMENT FOR ELECTRICAL POWER APPLICATIONS

ANNUAL REPORT FOR FY 1992

Abstract

Development of useful high–critical–temperature (high–T_c) superconductors requires synthesis of superconducting compounds; fabrication of wires, tapes, and films from these compounds; production of composite structures that incorporate stabilizers or insulators; and design and testing of efficient components. This report describes the technical progress of research and development efforts aimed at producing superconducting components that are based on the Y–Ba–Cu, Bi–Sr–Ca–Cu, Bi–Pb–Sr–Ca–Cu, and (Tl,Pb)–(Ba,Sr)–Ca–Cu oxide systems. Topics discussed are synthesis and heat treatment of high–T_c superconductors, formation of monolithic and composite wires and tapes, superconductor/metal connectors, characterization of structures and superconducting and mechanical properties, fabrication and properties of thin films, and development of prototype components. Collaborations with industry and academia are documented.

1 Introduction

The superconductor program at Argonne National Laboratory (ANL) includes development of both bulk and film processing, and is directed toward improving the properties of high-critical-temperature (high-T_c) superconductors, developing processing methods for producing commercial conductors, and fabricating and testing prototype conductors. Team relationships with industrial and academic partners are integral to this program. The principal objective of the ANL program is to develop methods to fabricate and use structurally reliable high-T_c superconductors for the generation, transmission, and storage of electrical energy. Ceramic processing and joining techniques are being developed to provide useful conductors from one or several of the high-T_c superconductors. Work has focused on superconductors that are based on yttrium-barium-copper oxide (YBCO), bismuth-strontium-calcium-copper oxide (BSCCO), lead-doped bismuth-strontium-calcium-copper oxide (PBSCCO), and thallium-barium-calcium-copper oxide (TBCCO). Primary emphasis is on the Bi-based superconductors.

Monolithic and composite conductors in the form of wires, tapes, films, or other shapes must meet several requirements. For most applications, the conductors must be capable of carrying large currents in the presence of large magnetic fields and they must be strong, flexible, and chemically and cryogenically stable. Potential applications for such conductors include transmission lines, motors, generators, transformers, magnetic-energy storage devices, and electronics (Wolsky et al., 1987). The principal impediments to the use of bulk high-T_c superconductors are low critical current density (J_c), poor mechanical properties, and lack of continuous lengths with uniform properties. Processing methods for improving all of the conductors have been and continue to be developed. The goals of ceramic fabrication include promoting high conductivity by obtaining phase-pure materials and imparting favorable grain alignment, maximizing flux pinning through microstructural control, and increasing flexibility and reliability by minimizing microstructural flaws and optimizing the strength and toughness of each material.

This report reviews the technical progress and status of (1) synthesis and heat treatment of high-T_c superconductors; (2) formation of monolithic and composite wires, tapes, and thick films; (3) characterization of superconductor/metal interfaces; (4) characterization of superconducting and electrical properties, microstructures, and mechanical properties; (5) fabrication of thin films and evaluation of their properties; and (6) fabrication and testing of prototype superconducting devices. Interactions with industry and academia are also documented.

2 Technical Progress in 1991–1992

2.1 Synthesis and Heat Treatment

2.1.1 Y-Ba-Cu-O System

In the previous period, substantial effort was concentrated on synthesizing large batches of phase-pure orthorhombic YBCO powders from Y_2O_3, $BaCO_3$, and CuO precursors. Reduced-pressure calcination at ≈800°C was used to prepare the superconducting powders. During calcination, $BaCO_3$ decomposes and then reacts to form intermediate compounds that react further to form the YBCO superconductor. The formation of intermediate compounds during calcination was monitored by X-ray diffraction (XRD), scanning electron

microscopy (SEM), and thermal analysis of precursor powders heated to various temperatures up to 800°C. The reaction passes through the formation of $BaCuO_2$, $BaCO_3$, $Y_2Cu_2O_5$, and Y_2BaCuO_5 (211). The YBCO phase begins to form at temperatures as low as 725°C under an O_2 pressure of 2.6×10^2 Pa. (Balachandran et al., 1991, 1992c).

The quality of the superconductor powder produced by reduced-pressure calcination is better then that of conventionally processed powders (Balachandran et al., 1992b). Special care is taken to keep the C content of the powder low, because C has an appreciable solubility in YBCO (Lindemer et al., 1990), and its presence can degrade superconducting properties.

Sintering studies of YBCO have continued. Microstructures of monoliths have been optimized by controlling O_2 partial pressure (pO_2) and heat treatment. Plastically extruded YBCO wires (1.1 mm diameter) were sintered at various pO_2 levels and temperatures. The resulting densities and grain sizes of the YBCO wires are shown in Table 1. For a pO_2 of 0.1 MPa, the density of YBCO wires increased from 79 to 98% of theoretical when sintering temperature was increased from 910 to 950°C. However, this density increase was associated with a corresponding increase in average grain size from 4 to 23 μm. The increased grain size had a deleterious effect on the strength of YBCO, which declined from 120 MPa for specimens with an average grain size of 4μm after sintering at 910°C, to 83 MPa for specimens with an average grain size of 23 μm after sintering at 950°C. This confirms the inverse dependence of strength on grain size. The effect of increasing strength with decreasing grain size was clearly evident in the fact that, despite their lower average density (79%), specimens that were heat treated at 910°C (producing a smaller grain size of ≈4 μm) were stronger than those heat treated at 950°C (having a larger grain size of ≈23 μm). Therefore, we initiated an effort to further increase strength by increasing density while maintaining a fine-grained microstructure. To this end, specimens were sintered at various pO_2 levels to evaluate the effects of pO_2 on the sintering kinetics of YBCO (Singh et al., 1992).

Table 1. Dependence of density, grain size, and strength on heat treatment

Temperature and Time (°C/h)	pO_2 (MPa)	Density (% theo.)	Average Grain Length (μm)	Strength (MPa)
910/10	0.1	79%	≈4.0	120 ± 10
925/10	0.1	90%	6.0	141 ± 09
935/12	0.1	96%	16.0	91 ± 07
935/20	0.1	96%	16.5	95 ± 06
950/20	0.1	98%	23.0	83 ± 05
910/10	0.05	70%	3-5	N/A
910/10	0.001	91%	3-5	191 ± 07
910/10	0.0001	94%	3-5	72 ± 19
910/10	0.000042	83%	3-5	73 ± 38

As seen in Table 1, a decrease in pO_2 from 0.1 to 0.001 MPa resulted in a corresponding increase in density from 79 to 91% of theoretical for specimens sintered at 910°C for 10 h, while grain size remained at 3–5 μm. This increase in density further increased strength from 120 to 191 MPa. The decrease in grain size had no adverse effects on superconducting properties. It is believed that the increase in density with a decrease in pO_2 is the result of enhanced sintering kinetics (Chen et al., 1989), probably due to both increase in defect concentration and decrease in activation energy of the rate-controlling species.

However, a larger reduction in pO_2 (<0.0001 MPa) resulted in a corresponding decrease in density as a result of second-phase impurities precipitated due to thermodynamic instability of YBCO at very low pO_2's (Bormann and Nölting, 1989, Singh et al., 1992). On the other hand, specimens sintered for 10 h at 910°C and pO_2 of 0.0001 MPa showed relatively low strength, despite having high density (94%) and small grain size. Although the specimens did not show signs of bulk decomposition under these conditions, a possibility of local decomposition could not be discarded. This local decomposition may have resulted in larger critical flaws, and hence decreased strength. Therefore, it is believed that pO_2 = 0.0001 MPa represents a borderline at which thermodynamic instability begins.

2.1.2 Bi-Sr-Ca-Cu-O System

As reported previously, we now synthesize a powder of the $Bi_2Sr_2CaCu_2O_x$ (2212) phase that is shown to be phase pure by XRD and differential thermal analysis (DTA). Low-pressure calcination is used to increase reaction kinetics and remove C, but higher pressure O_2 is needed to form the desired 2212 phase (Bloom et al., 1991). This powder is now being used to fabricate tapes and thick films (Poeppel et al., 1991).

Efforts to synthesize phase-pure $(Bi,Pb)_2Sr_2Ca_2Cu_3O_x$ (2223) with a T_c of ≈110 K have been completed. The kinetics of formation of the 2223 phase are extremely slow, but they can be accelerated significantly by substituting lead for bismuth (Shi et al., 1989). Some investigators claim that excess calcium and copper also enhance the kinetics (Shi et al., 1989; Koyama et al., 1988), but analysis of multiphase samples by electron microprobe has suggested that the 2223 phase may be an alkaline-earth-deficient relative to the ideal composition (Hong et al., 1990). In the most recent ANL study, a $Bi_{1.8}Pb_{0.4}Sr_2Ca_2Cu_3O_x$ mixture was prepared by ball milling Bi_2O_3, PbO, $SrCO_3$, $CaCO_3$, and CuO powders in isopropanol for 16 h. The slurry was pan dried and ground to a mean particle size of ≈4 μm. The resulting powder was separated for three calcination schedules, each of which included an initial heating at 400 Pa in flowing O_2, followed by an ambient-pressure anneal in flowing CO_2-free air. Various phase yields were produced by altering the final heat treatment. A powder that was almost phase-pure 2223 by XRD evaluation was synthesized by heating to a temperature just below that needed for formation of appreciable liquid phase. The final segment of the schedule was 100 h at 855°C in dry, CO_2-free air (Kaufman et al., 1993).

Subsequent processing of the highly pure 2223 and other, less-pure powders led to the conclusion that in-situ reactions are best for the formation of 2223 conductors. For example, for Ag-clad 2223 tapes, phase-impure powders produced higher J_c values than did phase-pure powders (Balachandran et al., 1992a; Kaufman et al., 1993). Therefore,

efforts to synthesize phase-pure 2223 powders have been shifted to controlled processing of phase-impure powders. The results of this work will be discussed in Section 2.2.2.

2.1.3 Tl-Ba-Ca-Cu-O System

Work has continued on the fabrication of Ag-clad $TlBa_2Ca_2Cu_3O_x$ tapes and wires (Goretta et al., 1992b). This composition has a T_c of ≈120 K and has an advantage in that little Tl is evolved during heating (Goretta et al., 1990a). In addition, the flux-pinning characteristics of the one-Tl-layer compound flux-pinning characteristics are superior to those of the Bi-Sr-Ca-Cu-O and two-Tl-layer compounds (Kim et al., 1991; Poeppel et al., 1991). Small batches of high-quality powder are required for the conductor work. Two compositions are now under examination: $TlBa_2Ca_2Cu_3O_x$ (1223) and $Tl_{0.5}Pb_{0.5}Ba_{0.4}Sr_{1.6}Ca_2Cu_3O_x$ (doped 1223). The latter compound has a shorter c axis and should therefore exhibit better inherent flux pinning (Kim et al., 1991).

For pure 1223, Tl_2O_3 was mixed with calcined Ba-Ca-Cu oxides, placed in a Pt crucible, and fired in flowing O_2 at ≈900°C. Silver foil was used to seal the crucible. The powders were highly phase-pure by XRD and DTA. Scanning and transmission electron microscopy (SEM and TEM) examinations revealed, however, that small particles of CaO and $BaCuO_2$ were present in the powders. The impurity phases constituted <5% of the total. Because no Tl was present in the second phases, and no free Tl oxides were observed, it was surmised that a Tl deficiency may be responsible for much of the nonsuperconducting mass (Goretta et al., 1992a). Future efforts will concentrate on addition of excess Tl_2O_3 to compensate for that lost during firing.

Synthesis of the doped 1223 compound is being pursued in collaboration with staff members of Los Alamos and Sandia National Laboratories (LANL and SNL). The work is in a preliminary stage, but clear trends have emerged. Barium and Pb have a strong tendency to form a stable $BaPbO_3$ compound. To minimize the $BaPbO_3$ content of the final powder, the staff at SNL have synthesized, by coprecipitation, a precursor that contains all of the non-Tl constituents. Because the cations are distributed on a very fine scale, subsequent heat treatment promotes formation of complex oxides at the expense of $BaPbO_3$. The doped 1223 powders produced to date are ≈90% pure and have T_c values up to 117 K. Additional work is in progress at all three laboratories. A conclusion to these synthesis efforts is expected by mid-1993.

2.2 Production of Bulk Conductors

2.2.1 Monolithic Conductors

Wires

Plastic extrusion can yield long lengths of high-T_c superconductors. Effective removal of organic constituents used in extrusion is required, however. In previous reports, the benefits of low-pressure firing for this purpose were described (Poeppel et al., 1990; 1991). The removal of organics is a complicated process. To optimize the removal of organics from large superconductor pieces, the effects of the following have been analyzed for the heat treatment of multilayer YBCO coils: total pressure in the furnace, O_2 flow rate, heat conduction, and diffusion of volatile components (Cha et al., 1992).

Modest J_c values have been achieved for monolithic and multilayer YBCO wires (Poeppel et al., 1992). These wires will probably be of use only for low-J_c applications such as current leads (Wu et al., 1991). Much of our extrusion work is now focused on coextrusion of Ag-clad composites. Extruded wires were, however, used to demonstrate of the feasibility of producing a 1-m-long ceramic superconductor assembly capable of 1000-A operation at 77 K. YBCO superconductors with particulate Ag additions in the form of rods, tubes, and flat strips were produced by extrusion and subsequent burnout of organic additives and sintering. Critical current densities as high as 300 A/cm^2 were realized over the sample length, but were only seldom achieved. In addition, the cross-sectional areas of the wires were not large. We developed a method of cold isostatic pressing of 1-m-long, 10-mm-diameter rods that required relatively little addition of organic material in the forming process. After sintering, these rods were superior in strength and total current. The problem of wide batch-to-batch variation in electrical performance was not completely overcome. A minimum criterion of 50 A/rod in a 40-G ambient magnetic field was adopted, and a set of rods was produced for the assembly. The results of pulse tests indicated that the assembly will perform successfully at 77 K in a future test at 1000 A continuous current.

Melted Rods and Pellets

Low-temperature melt-growth processing has been developed to fabricate ≈4-cm-diameter, 1.3-cm-thick pellets for flywheel applications. The low-temperature processing was made possible by addition of submicron-sized Y_2BaCuO_5 (211) particles to YBCO powder prior to melt processing. The maximum processing temperature was ≈1050°C, compared to ≈1400°C used in conventional quench-melt-growth processing (Murakami et al., 1989). The relatively low processing temperature used in our work minimizes contamination from crucible materials. The YBCO pellets fabricated by this technique have been used to make a dozen prototype flywheel units and have been supplied to various utility companies (Weinberger et al., 1990, 1991). These melt-processed pellets are the basis for the formation of a flywheel consortium among various utilities.

In working with 211-added YBCO, it was found that flux pinning could be significantly enhanced by introducing fine 211 precipitates into a YBCO matrix. These results agree well with those reported by Murakami et al. (1989). The increased flux pinning effects were attributed to defects associated with the 211 and magnetic pinning from the 211 particles in the YBCO. Although the average dimension of the pinning centers (≈0.5 μm) was much larger than the coherence lengths of YBCO, flux pinning could still be effective, possibly because of faults near the 211 or because the 211 particles were numerous and served as volume pins (Shi et al., 1989; Sengupta et al., 1992).

2.2.2 Composite Conductors

Processing of high-T_c superconductors in Ag tubes has produced several reports of J_c values greater than 10^4 A/cm^2 at 77 K and greater than 10^5 A/cm^2 at 4.2 K (Jin and Graebner, 1991). Advantages of powder-in-tube processing include high green densities, which obviate the use of high sintering temperatures; protection of the superconductor from atmospheric exposure; and possible stabilization of the superconductor by the resultant metallic sheath. Ag is used for the sheath because of its chemical compatibility with the high-T_c superconductors (Meyer et al., 1989).

Wires and Tapes

At ANL, research has included swaging, drawing, pressing, and rolling operations and tape casting (Poeppel et al., 1991; 1993). Results throughout the world indicate that the J_c for sintered YBCO forms is unlikely to exceed $\approx 10^4$ A/cm^2 at 77 K and drops rapidly with applied field (Goretta and Shi, 1992). The feasibility of melt-texturing YBCO in an alloy sheath was investigated. YBCO was processed on 90% Ag/10% Pd substrates. This alloy has a melting temperature of ≈1000°C, which is higher than the 980°C melting point of YBCO in 1% O_2 (Risch et al., 1991). Melt-processing in 1% O_2 produced a superconductor core with large aligned YBCO grains. However, phases rich in Ba and Cu were formed along the interface and the T_c of the core was reduced ≈3 K because of the presence of the Pd. The conclusion from this work was that use of Ag/Pd alloys offers promise for possible melt-texturing of YBCO in a metallic sheath.

We fabricated Ag-clad 2212 BSCCO tapes with high transport J_c values at 4.2 K. However, these J_c values have been only attainable at ≈75–77 K. The highest J_c was 10^5 A/cm^2, which did not decrease in a field of 60 mT (Wu et al., 1993). Magnetization studies indicated that J_c should remain high up to a temperature of ≈25 K. Systematic study of processing variables indicated that rolling at 10% reduction per pass led to higher J_c values (Fig. 1) and that an intermediate partial-melting heat treatment was essential for good superconducting properties. X-ray diffraction (Wu et al., 1991) has indicated that J_c is correlated with texture. Current work is focused on reducing the size and concentration of the second phases that form during partial melting and on increasing T_c.

We have fabricated Ag-clad 2223 tapes from multiphase powders that sinter reactively in-situ to form 2223. The kinetics of 2223-phase formation and its relationship to microstructure and electrical properties were studied (Kaufman et al., 1993). The primary focus of this study was to determine the optimal thermomechanical process conditions that are necessary to obtain textured microstructures and high J_c values (10^4 A/cm^2 at 77 K).

Three $Bi_{1.8}Pb_{0.4}Sr_2Ca_2Cu_3O_x$ powders were calcined to varying degrees of phase purity (Kaufman et al., 1993). The primary phases were 2212, $Bi_2Sr_2CuO_x$ (2201), and 2223 for respective A, B, and C powders. Data obtained by DTA in air revealed two endotherms, between 830°C and 870°C, for all of the powders (Fig. 2). Subsequent heat treatment for

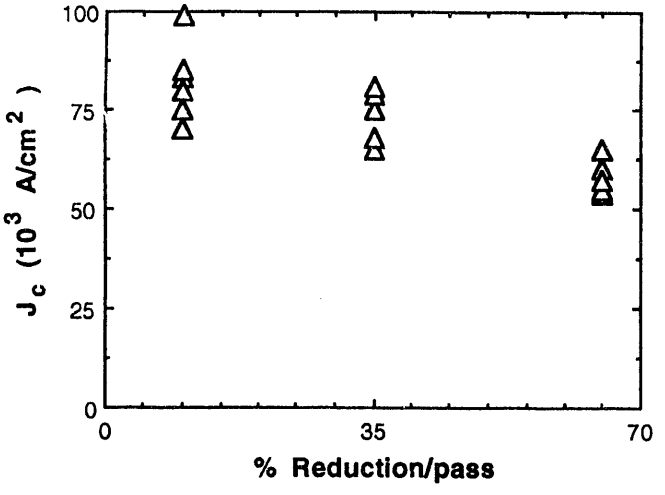

Fig. 1.
Transport J_c at 4.2 K as a function of % reduction during rolling

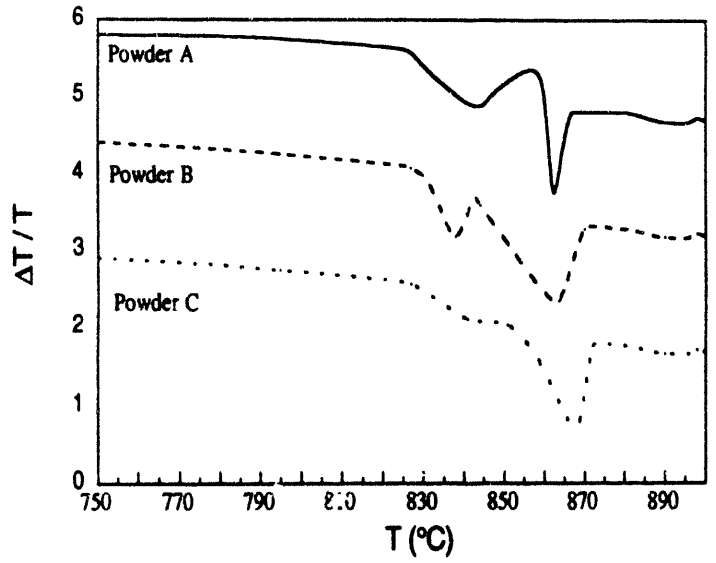

Fig. 2.
Curves obtained by DTA of calcined powders mixed with 20% Ag

powder-in-tube specimens was carried out in the region of the first endotherm (830–857°C). Initial experiments were aimed at determining the optimal processing temperature. Three-cm tapes were annealed for 50 h, cooled, uniaxially pressed for 5 s at 3.6 GPa to 22% reduction, and reannealed for 100 h. The pressing promoted reactivity and texture. The highest J_c value was found in powder A, which was heated near the first endotherm (Fig. 3). Significant J_c enhancement was observed for extended heat treatments (Fig. 4). Differential thermal analysis confirmed that the best heat treatment occurred slightly below the incongruent melting temperature of 2223. X-ray diffraction data indicated that J_c was related to phase purity; however, J_c was also related to microstructure. Highly aligned grains were developed during reactive sintering. Consequently, the most phase-pure starting powder was not the most desirable. The amount and type of liquid can be controlled by the phase type and distribution of the initial powder. We observed significant differences in the formation of the 2223 phase for powders calcined under the three different conditions.

The phase transformation behavior exhibited by 2223 wires produced in the ANL core program has been investigated by a combination of XRD and SEM. Heat treatments at 825°C in 7.5% O_2 were performed on two Ag-sheathed 2223 wires prepared from a batch of powder composed of 2212 + second phases. The powder in one of the wires (A) was vacuum calcined at 600°C prior to air calcining at 800°C; the powder in the second wire (B) was vacuum calcined at 750°C prior to air calcining at 800°C. The extent of transformation of A and B wire specimens to 2223 as a function of time (based on XRD analysis of quenched, peeled wire samples) is plotted in Fig. 5. Under the 825°C/7.5% O_2 heat-treatment conditions, A was a faster-reacting wire than B. In this particular case, we suspect that the different vacuum-calcining temperatures used on powder A and powder B altered the compositions of the alkaline-earth-cuprate second phases. Second-phase composition is known to have a pronounced effect on the rate and course of 2223 formation from 2212 + second-phase mixtures (Koyama et al., 1988; Kaufman et al., 1993).

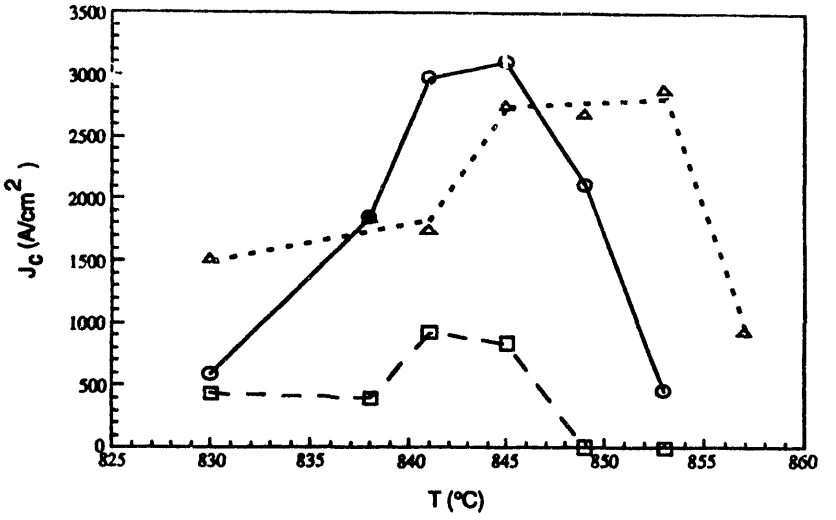

Fig. 3. Critical current density of (o) 2212, Tube A; (□) $Bi_2Sr_2CuO_x$ (2201) Tube B; and (Δ) 2223, Tube C as a function of 150-h annealing temperature

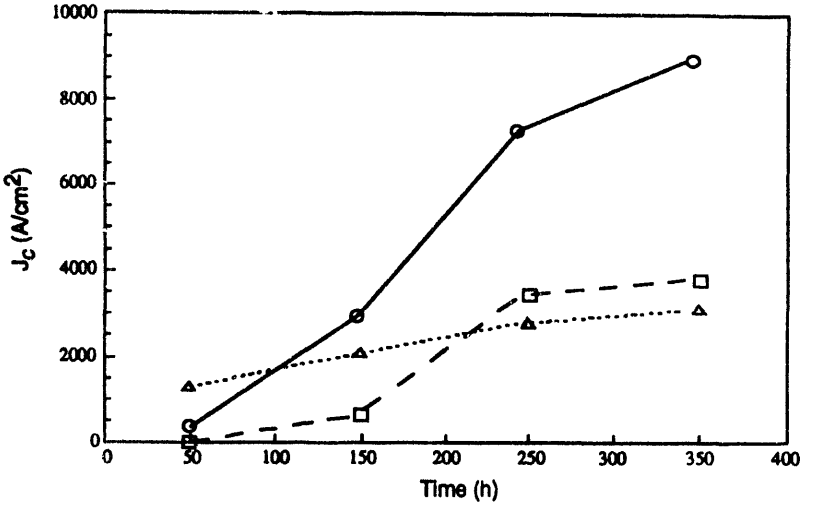

Fig. 4. Critical current density as a function of annealing time at 845°C. Tapes were pressed after 50, 150, and 200 h: (o) 2212, Tube A; (□) $Bi_2Sr_2CuO_x$ (2201), Tube B; and (Δ) 2223, Tube C.

The data in Fig. 6 were analyzed by the generalized equation for nucleated growth dynamics developed by Avrami, $C = 1-\exp[-kt^n]$, where C is the volume fraction of the product phase, t is time, and k is the reaction rate constant (Bamford and Tipper, 1969; Hulbert, 1969). A plot of $\ln[-\ln(1-C)]$ versus ln t should produce a straight line with slope n and intercept ln k. The value of n derived in this way provides insight about the nature of the rate-limiting process. The Avrami plots for the A and B results obtained at 825°C/7.5% O_2 exhibited reasonable conformance to straight lines with slopes (n) of 0.9–1.6, indicating a two-dimensional, diffusion-controlled reaction mechanism (Bamford and Tipper, 1969; Luo et al., 1992).

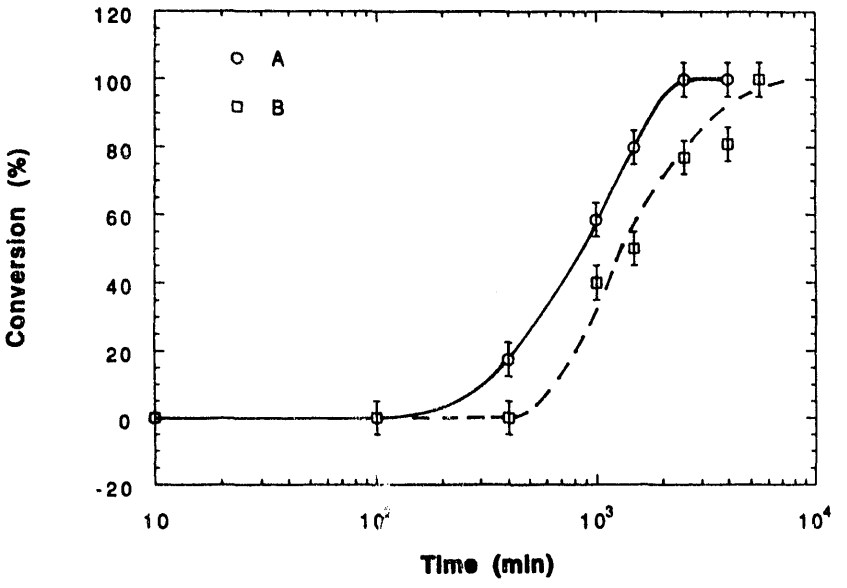

Fig. 5.
Percent conversion of Bi-2212 and second phases to 2223 versus heat treatment time at 825°C in 7.5% O_2 for wires made from A, 2212 and B, $Bi_2Sr_2CuO_2$ (2201)

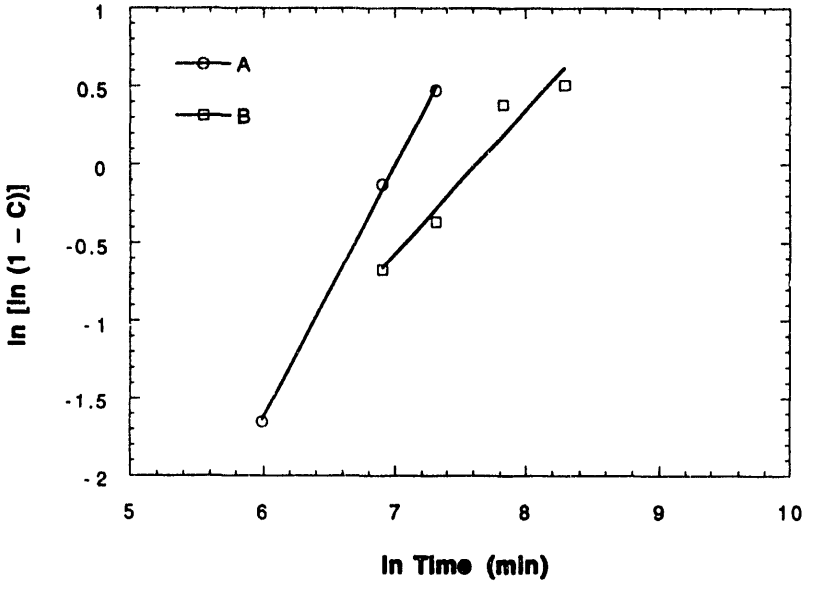

Fig. 6.
Avrami plot of conversion (to 2223) versus time data for wires A and B, obtained at 825°C in 7.5% O_2

In another series of 2223 phase-development studies, four Ag-sheathed wires (designated 5–8) containing powders in the 2223 stability field (Koyama et al., 1988), but with varying amounts of Bi, were heat treated in 7.5% O_2 at 825°C. Wires 5 and 6 contained powders with Bi = 1.8%. The powders in Wire 7 (Bi = 2.0%) and Wire 8 (Bi = 2.3%) were prepared by adding appropriate amounts of Bi_2O_3 to the powder used in Wire 6. The final calcination for the powder in Wire 5 was at 800°C in air for 24 h; final calcination of the powders for Wires 6–8 was at 855°C in air for 100 h.

Two heat treatments, one for 10 min and the second for 89 h, were completed on specimens of Wires 5–8. The purpose of the 10-min equilibration was to restore the natural powder phase crystallinity (which is degraded during drawing and rolling/pressing operations) without inducing any significant in-wire progression of the 2223-formation reaction. X-ray diffraction patterns obtained on peeled sections of the 10-min and 89-h wires gave the 2212/2223 ratios given in Table 2.

Table 2. Phases in 2223 wires heat treated as shown

Wire	% 2212/% 2223	
	10-min sample	89-h sample
5	100/0	0/100
6	50/50	18/88
7	44/56	9/91
8	33/67	16/84

X-ray diffraction also revealed the presence of 2201 phase (a known decomposition product of 2223), with the relative amount of 2201 increasing in the order B5 < B6 < B7 < B8. Texturing of the c axes of the 2223 phase in the 89-h samples was greatest for Wire 5, but all four wires exhibited substantial favorable texture.

The higher-temperature/longer-duration final calcination of the powders in Wires 6-8 (compared to that for Wire 5) generated significant quantities of 2223 in the as-loaded powders. However, even with major amounts of 2223 already present in Wires 6-8, less 2223 was produced and more 2212 remained after the 825°C/7.5% O_2/89-h heat treatment than was observed for Wire 5. It is not clear from this work whether increasing the Bi level slows 2223-formation kinetics or induces decomposition of 2223 to 2201, 2212, and Ca cuprates.

Images obtained by SEM of the cross sections of equilibrated wires (5-8) were promising. The powder in each wire was densely packed; second-phase crystallites were small, uniform in size, and well distributed, and there were very few quilted growths running into the Ag sheath. Energy-dispersive X-ray analysis of second-phase compositions, and postetch SEM studies of mounted wires (to study 2223 microstructure and texture) are in progress.

The presence of a liquid phase during powder-in-tube processing of 2223 is thought to be beneficial for several reasons. It enhances the kinetics of formation of 2223 (Hatano et al., 1988; Aota et al., 1989; Tsuchiya et al., 1989; Oh and Osamure, 1991), facilitates grain growth and alignment, and heals damage by mechanical processing (Yamada et al., 1991). Aota et al. (1989) reported that 2212 undergoes partial melting during formation of 2223 and that its partial-melting temperature can be lowered by decreasing O_2 pressure in the processing atmosphere. Grader et al. (1988) showed that increasing the Ca content in 2212 also lowers its melting point. Tsuchiya et al. (1989) found that 2223 can be produced if the melting point of 2212 is lower than that of 2223, and claim that the use of Ca-rich 2212 enhances formation of 2223. These reports suggest that the kinetics of 2223 formation, and perhaps its grain growth and alignment, can be controlled by the Sr and Ca content of 2212. To test this, mixtures of $Bi_{1.8}Pb_{0.4}Sr_{2-x}Ca_{1+x}Cu_2O_y$ and $Sr_xCa_{1-x}CuO_z$ have been processed by the powder-in-tube method to form the BSCCO 2223 phase inside an Ag sheath during heat treatment. Mixtures with an overall composition of $Bi_{1.8}Pb_{0.4}Sr_2Ca_2Cu_3O_v$ and x values of 0.0, 0.25, 0.50, 0.75, and 1.0 have been studied.

The starting phases, $Bi_{1.8}Pb_{0.4}Sr_{2-x}Ca_{1+x}Cu_2O_y$ and $Sr_xCa_{1-x}CuO_z$, were prepared from Bi_2O_3, PbO, $SrCO_3$, $CaCO_3$, and CuO. The powders were calcined first at reduced total pressure (6 h/750°C/≈400 Pa of O_2) to ensure complete decomposition of carbonates, then at ambient pressure in CO_2-free air (24 h at 840°C for $Bi_{1.8}Pb_{0.4}Sr_{2-x}Ca_{1+x}Cu_2O_y$ and 48 h at 900°C for $Sr_xCa_{1-x}CuO_z$) to produce nearly single-phase materials. The individual powders were characterized in terms of particle-size distribution, phase composition (by XRD), and melting behavior (by DTA). Powder mixtures, each with the overall composition $Bi_{1.8}Pb_{0.4}Sr_2Ca_2Cu_3O_v$, were made by milling the appropriate amounts of $Bi_{1.8}Pb_{0.4}Sr_{2-x}Ca_{1+x}Cu_2O_y$ and $Sr_xCa_{1-x}CuO_z$ in isopropanol. Ag was added (20 wt.%) to the mixtures to produce uniform melting in the BSCCO core. The powder mixtures were packed into Ag tubes, heated at reduced total pressure (6 h/700°C/≈260 Pa of O_2) to remove any absorbed moisture and/or CO_2, and sealed. The tubes were then drawn and rolled to a final tape thickness of 0.1 mm.

Samples ≈25 mm long were cut from the tapes and heat treated in air or 8% O_2. In air, the heat treatment temperatures were 835–845°C. In 8% O_2, the temperatures were 815–825°C. Thermomechanical processing of the tapes began with a 50-h anneal at the chosen heat treatment temperature, after which the tapes were uniaxially cold pressed at ≈2 GPa to give an ≈20% reduction in tape thickness. Following pressing, the tapes were annealed for an additional 100 h at a selected temperature. This process of pressing and annealing was repeated until heat treatment times reached 350 h. The J_c of each tape was measured at 77 K by the four-probe method in zero applied field with a 1-μV/cm criterion.

X-ray diffraction indicated that the $Bi_{1.8}Pb_{0.4}Sr_{2-x}Ca_{1+x}Cu_2O_y$ powders were nearly single-phase 2212, and that a trace of Ca_2PbO_4 was present for $x < 0.75$. For $x = 0.75$ and 1.0, substantial Ca_2PbO_4 and Sr_2PbO_4 and slight amounts of 2201 were present. The $Sr_xCa_{1-x}CuO_z$ powders were single-phase for $x > 0.25$, but contained $Sr_xCa_{2-x}CuO_3$ and CuO for $x = 0.25$ and 0.0.

Differential thermal analysis (Fig. 7) showed that the largest endotherm for the modified 2212, $Bi_{1.8}Pb_{0.4}Sr_{2-x}Ca_{1+x}Cu_2O_y$, presumed to result from partial melting, increased in air from ≈830°C for $x = 1.0$ to ≈865°C for $x = 0.0$. The DTA traces of the $Sr_xCa_{1-x}CuO_z$ (Fig. 8) also varied significantly, but not monotonically, with x. The DTA traces of the powder mixtures (Fig. 9), however, varied only slightly with x, suggesting that the reactions in the powder mixture were very fast. This conclusion is supported by SEM, which revealed very little second phase in the $x = 0.0$ mixture after only 50 h at 820°C in 8% O_2. Very large regions of second phase were seen when $x = 1.0$ under the same conditions, but the size of the second phase decreased dramatically after a total heat treatment time of 150 h (Poeppel et al., 1993).

In 8% O_2, the highest J_c at 77 K (≈3 x 10^4 A/cm^2) was obtained with the $x = 0.0$ mixture after 350 h at 820°C. J_c for the other samples under the same conditions ranged down to 0.8 x 10^4 A/cm^2 for the $x = 1.0$ sample. The highest J_c in air (1.3 x 10^4 A/cm^2) was also obtained with the $x = 0.0$ sample.

The 2223 Bi-Sr-Ca-Cu-O superconductor also forms the basis of a joint program between ANL and Intermagnetics General Corporation (IGC). The goal of this program is to produce long and uniform lengths of high-quality composite conductors that exhibit excellent mechanical and physical properties for commercial operation at 35 K in applied fields up to 2 T. The initial focus of the program is to extend powder-in-tube processing to

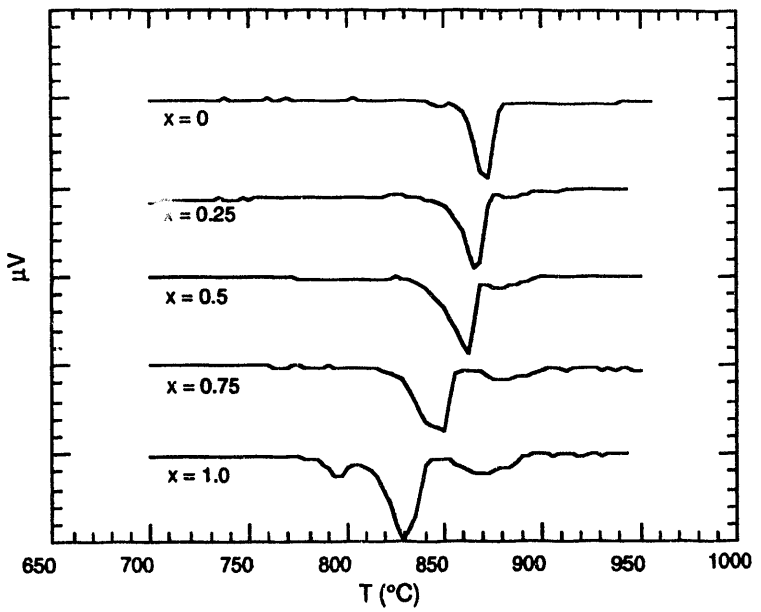

Fig. 7.
DTA traces for Bi-2212 with various values of x

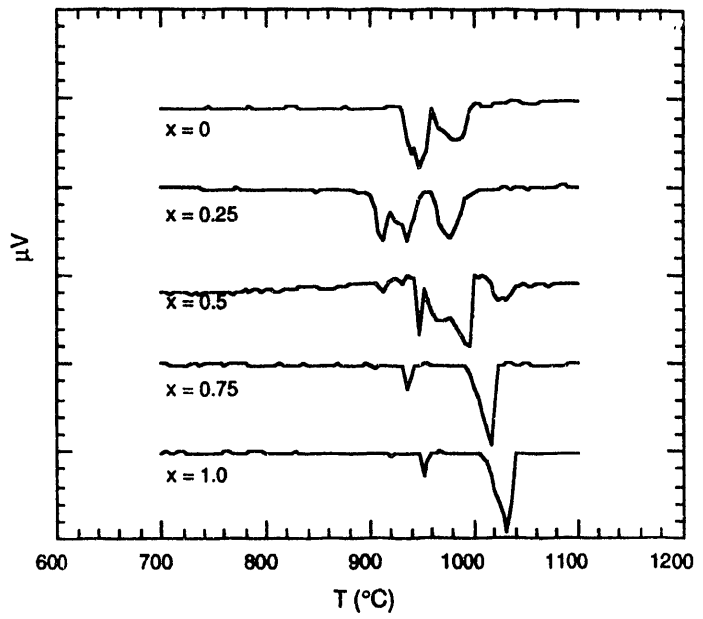

Fig. 8.
DTA traces of $Sr_xCa_{1-x}CuO_z$ with various values of x

yield conductors with practical current densities in lengths up to 10 m. The longer term focus will be on developing manufacturing technology for lengths of conductor >100 m for incorporation into large-scale energy-related applications. This research encompasses all phases of conductor fabrication, from powder synthesis and wire/tape forming by the powder-in-tube technique to identification of heat-treatment conditions to optimize superconducting properties.

Reactive sintering of Ag-clad 2223 tapes is now used. As in ANL in-house work, we have found that, to obtain good microstructures and high J_c values, an in-situ reaction, with the formation of a transient liquid that is consumed during the final heat treatment, must occur between constituent phases. Transient liquid forms from low-melting eutectics in the multiphase precursor powder packed into the Ag tubes. The liquid phase facilitates

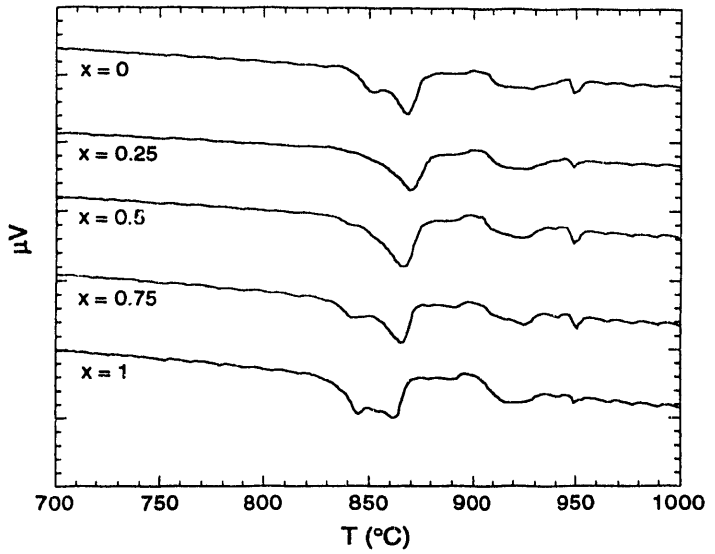

Fig. 9.
DTA traces for $(Bi,Pb)_2Sr_2Ca_2Cu_3O_x$ with various values of x

grain growth and texturing and heals cracks formed during mechanical processing. Inasmuch as the liquid phase plays a central role in the processing of tapes, we seek to optimize its effect on the microstructure and properties of 2223 by manipulating the composition of the liquid, its amount, and the temperature at which it is formed.

The multiphase precursor powders are prepared from Bi_2O_3, PbO, $SrCO_3$, $CaCO_3$, and CuO by calcining in the temperature range of 800–850°C for ≈50 h (Balachandran et al., 1988). The prepared powders are characterized, packed into Ag tubes, and fabricated into tapes. The highest transport J_c values were obtained with repeated thermomechanical working (initial heat treatment of tapes followed by mechanical pressing and another sintering and repeating this process) of short lengths of tapes. The J_c was affected by the degree of mechanical deformation that occurs during processing. Major accomplishments to date have been (1) in short samples, $J_c \approx 4 \times 10^4$ A/cm^2 was achieved at 77 K , 0 T; $J_c > 2 \times 10^4$ A/cm^2 was achieved at 35 K and 2 T with H // c direction; (2) samples were measured in applied fields to 3 T at 77 K and in pumped liquid N_2 at 64 K; (3) at 77 K in fields <1 T, the orientation of the field had no effect on J_c; and (4) an order-of-magnitude improvement in J_c was achieved at 2 T in the H // a-b direction with a temperature decrease from 77 to 64 K.

Pancake coils of 1-m-long tape conductors exhibited $I_c \approx 15$ A at 77 K. This corresponds to a J_c 77 K of ≈7.8 x 10^3 A/cm^2, which is approximately 80% of the average value of the short sample from that particular batch. I_c was ≈60 A ($J_c \approx 3 \times 10^4$ A/cm^2) at 4.2 K in applied field of 13 T. An 11.8-m coil exhibited a J_c of ≈3.5 x 10^3 A/cm^2 at 77 K in zero applied field. The J_c-versus-applied-magnetic-field (H // a-b) data at various temperatures for representative tapes are shown in Fig. 10 (Balachandran et al., 1992a; Haldar et al., 1992).

Ag-clad $TlBa_2Ca_2Cu_3O_x$ (TBCCO 1223) wires and tapes have been fabricated. The wires carried 10–13 A at 77 K and 30–50 A at 4.2 K. The highest J_c values have been 4 x 10^3 A/cm^2 at 77 K and ≈2 x 10^4 A/cm^2 at 4.2 K. The response to a magnetic field has been similar to that of a BSCCO superconductor. Currently, the Ag-clad TBCCO tapes appear to have a weak-link problem. Because solid-state sintering could not remove the weak links,

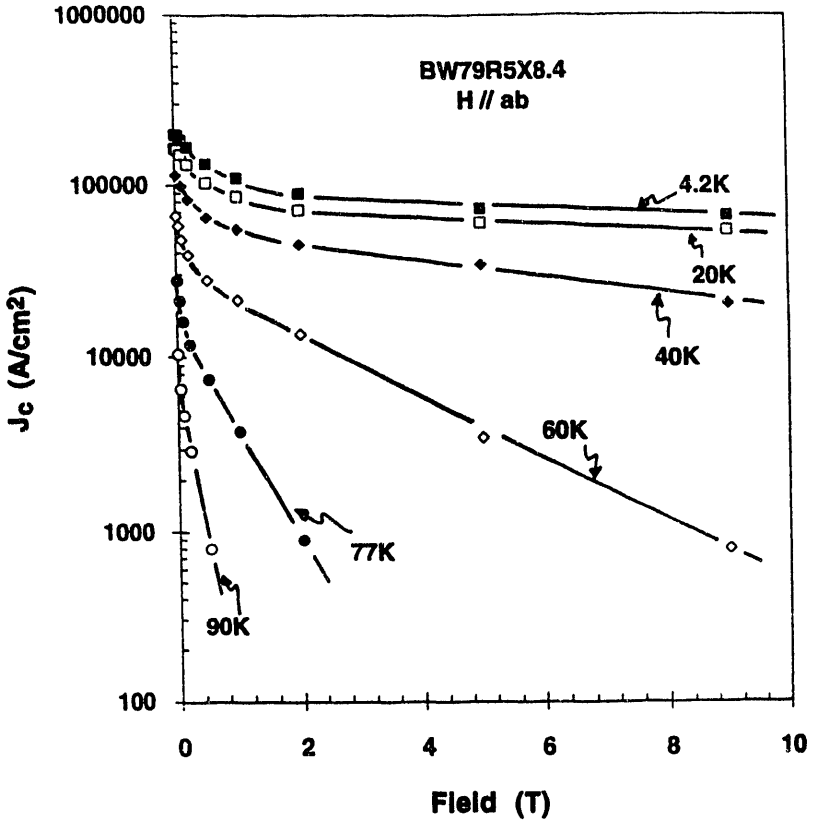

Fig. 10. Transport J_c versus applied magnetic field for 2223 tapes

various partial-melting heat treatments were used. These succeeded in producing well-aligned grains in some places, but the overall texture of the wires remained poor. The interaction between the TBCCO 1223 and the Ag sheath was severe. We are now attempting to reduce the processing temperature so that the interactions are minimized. In addition, we are trying to use the reactive in-situ formation of the 1223 phase in an approach similar to that used for the 2223 PBSCCO compound. This approach has demonstrated substantial promise (Seido et al., 1993).

2.2.3 Thick Films

Thick films of 2223 BSCCO were fabricated by applying onto Ag substrates, a highly viscous slurry composed of a superconducting powder and an organic solvent. As with the previous work with 2212 thick films (Poeppel et al., 1991), a dispersant was used to deflocculate particles and enhance rheological properties. The painted substrates were then dried. The specimens were subsequently pressed and fired at various temperatures and characterized by SEM, XRD, and current transport. Although the major phase present in all films was 2223, substantial 2212 was also present. Some c-axis texture perpendicular to the plane of the thick film was confirmed. Transport J_c values have been difficult to obtain because of the low resistivity of Ag and the relative thinness of the film. Work to improve alignment and phase yield is in progress.

2.3 Properties of Bulk High-T_c Superconductors

2.3.1 Characterization Methods

Ceramic superconductor samples produced by ANL are characterized to help guide improvement of the chemical formulations and the forming and processing procedures. High-T_c products fabricated by ANL for use by others are also characterized to evaluate product performance. The property of primary interest is the DC transport critical current value (I_c) of the sample or the J_c, measured as a function of the intensity of an applied magnetic field. Selected samples are tested to find the critical temperature, AC resistance, structural defects, or strength of the diamagnetic response, remanent field strength, and magnetic-shielding performance.

2.3.2 Screening Tests

Critical current density tests have continued at an average rate of ≈110 new samples each month. Substantial differences among batches of bulk material or formed products necessitated continual screening. The standard four-point resistance method was used with a 1-μV/cm J_c criterion. Results are discussed in this report.

Pulsed currents at low duty cycle are used to test the superconductors when continuous currents would cause excessive heating of the connecting leads and/or contacts to a sample or when the current required is greater than the capacity of the available supplies of continuous current. These conditions were frequently encountered during this reporting period, becasue we tested samples that exhibited critical currents >100 A. Also, our pulsed-current facility provided the capability to test an assembly of several such samples, which were connected in parallel for a transport-current demonstration project.

2.3.3 Facility Upgrades and Test Results

For such tests, a 1000-A pulsed-current system was assembled and applied. The design of the sample-support probe segregates and shields the voltage-monitoring leads from the current leads and locates the measurement ground connection near or on the sample. The current source is ground-isolated. With this arrangement, the common mode signal is negligible. Also, the effective level of ambient electrical noise is reduced to <1μV input equivalent when the probe is used with low-pass filtering consistent with the application of current pulses 100 ms or greater in length. Smaller pulse lengths can be used when a sample length much greater than 10 mm permits the use of a reduced-voltage-measurement sensitivity. At the 1000-A level, 250-ms-long square wave pulses can be applied at a 1% duty cycle.

The pulser was used to test YBCO samples of large cross-sectional area (1 cm^2) at 77 K and powder-in-tube and melt-textured BSCCO superconductors with high J_c values at 35, 20, and 4.2 K. The measured J_c values are given elsewhere in this report.

A new gas-flow cryostat containing a 7-T superconducting magnet was installed in the electrical evaluations laboratory of the ANL Ceramics Section. Samples of relatively large diameter can be accommodated in the 60-mm-diameter sample space located in the 76-mm-diameter, 170-mm-long bore of the magnet. The sample temperature can be controlled in the range from that of liquid He to room temperature. The sample-holding

probe can deliver current pulses up to several hundred amperes to samples having low contact resistance. The system has been used to find (1) J_c for superconductors at 4.2 and 20 K in fields of 0–2 T and (2) T_c above 77 K.

Past work has shown the low resistance of Ag/superconductor interfaces that are formed by applying Ag powder to small-area (≈5 mm^2) surfaces of YBCO–Ag conductors prior to sintering. Recently, this finding was verified with larger surface areas (≈0.5 cm^2) and at higher current (80 A). The overall resistance at 77 K of one lapping pair of such contacts, including a thickness of solder between them, was only 0.5 μΩ; the specific interfacial resistivity, derived by subtracting the contributions of the metallic layers and accounting for the configuration and size of the lap joint, was 64 $n\Omega\text{–}cm^2$. In comparable tests, the overall resistances were greater but within a factor of two of that noted above.

A small resistance to alternating current flow is displayed by high–Tc superconductors, even at currents well below the DC J_c, as reported previously (Poeppel et al., 1991). This resistance is associated with the magnetic hysteresis of the material, and, as found here earlier, the energy loss per cycle of current is rather independent of the AC frequency up to at least 400 Hz. In tests of selected 1–mm–diameter YBCO wires, the AC dissipation was equal to that produced by DC at the 1 μV/cm critical level when a 50–Hz test current was 67–80% of the DC critical value.

During this reporting period, the study of AC resistance in superconductors produced at ANL was continued in collaboration with Prof. M. Marinelli of the University of Genoa, Italy. Magnetic–hysteresis of polycrystalline, untextured superconductors was measured. Results correlated well with those of AC transport current tests and supported the previous findings. We developed a theoretical analysis that used a phenomenological critical–state model with two phases that accounted quantitatively very well for the results of the two kinds of measurements. The model suggests that AC loss may be reduced if superconductor diameter is reduced and the reduction is compensated for by the use of several parallel superconductors. Continuing work will test this conclusion and extend the loss measurements to textured materials and materials with greater levels of flux pinning.

A brief study was conducted of the effects of AC field frequency on the effectiveness of degaussing in the removal of remanent fields from both sintered and melt–processed superconductors. As expected, the fields were removed as a function of degaussing field strength, with no first–order effect of frequency up to 2 kHz, the highest value tested.

2.3.4 Mechanical Properties

Mechanical–property research has continued. In general, the fracture toughness (K_{IC}) and strength of monolithic bulk high–T_c superconductors are poor. Previous efforts led to improvements in the K_{IC} of YBCO from ≈1.5 $MPa(m)^{0.5}$ to 4.5 $MPa(m)^{0.5}$; in its strength from ≈100 MPa to ≈230 MPa. K_{IC} was increased by additions of particulate Ag and 211–coated ZrO_2. Strength was increased by low–pressure sintering methods designed to minimize grain growth while maximizing density (Poeppel et al., 1990; Singh et al., 1992).

Effects of Ag additions on thermal shock and delayed failure

The effects of Ag additions on delayed failure and resistance to thermal shock of YBCO superconducting wires have been evaluated. YBCO develops residual internal stresses during fabrication due to expansion and modulus anisotropy, which may promote subcritical growth of preexisting flaws and result in delayed failure (Singh et al., 1989). Furthermore, during service, engineering components made from YBCO are expected to be subjected to repeated thermal cycling, which may result in thermal fatigue and possible premature failure. Resistance to thermal shock, thermal fatigue, and delayed failure can be improved by increasing strength and fracture toughness (Singh et al., 1993). Ag has proved to have beneficial effects on mechanical properties of YBCO (Singh et al., 1989). Therefore, an evaluation of the effects of Ag additions on basic mechanical properties and resistance to thermal shock and delayed failure was conducted.

Table 3 shows mechanical-property data of extruded wires of YBCO and YBCO/Ag composites. Addition of 15 vol.% Ag increased the strength and fracture toughness of YBCO from 191 to 225 MPa and 1.8 to 3.1 MPa(m)$^{0.5}$, respectively. As discussed by Singh et al. (1992,1993), these improvements in mechanical properties are believed to be due to (1) relaxation of residual stresses in YBCO resulting from grain anisotropies, (2) introduction of compressive stresses in the YBCO matrix as a result of thermal mismatch between YBCO and Ag phase, and (3) increased resistance to crack propagation as a result of crack pinning, deflection, and bridging.

Table 3. Properties of extruded wires

Specimen	Strength (MPa)	Fracture Toughness [MPa(m)$^{0.5}$]
YBCO	191 ± 30	1.8 ± 0.4
YBCO-15 vol.% Ag	225 ± 06	3.1 ± 0.2

To evaluate thermal-shock resistance of YBCO and YBCO/15 vol.% Ag wires, specimens were first quenched in liquid N_2 at various quenching rates. The quenching rates were measured approximately by counting elapsed time during temperature change from room temperature to 77 K (Singh et al., 1993). Subsequently, the specimens were removed from the liquid N_2 and were allowed to warm to room temperature. The thermal-shock damage was evaluated by measuring J_c before and after each thermal cycle.

The variation in J_c of YBCO and YBCO/Ag wires (quenched at a rate of 15°C/s) as a function of thermal cycles is shown in Fig. 11. The J_c values of both YBCO and YBCO/Ag wires decreased with increasing number of thermal cycles. In general, thermal stresses induced during thermal cycling may cause microcracking. The microcracks, as well as preexisting flaws, may increase in size by a fatigue process during repeated thermal cycling. The cracking reduces J_c.

The relative decrease in J_c with increasing number of thermal cycles was smaller for YBCO/Ag composites than for monolithic YBCO. For example, the value of retained J_c of YBCO/Ag composites after 10 thermal cycles was 1.6 times higher than that of the monolithic YBCO specimen. This improved performance of YBCO/Ag composites may be

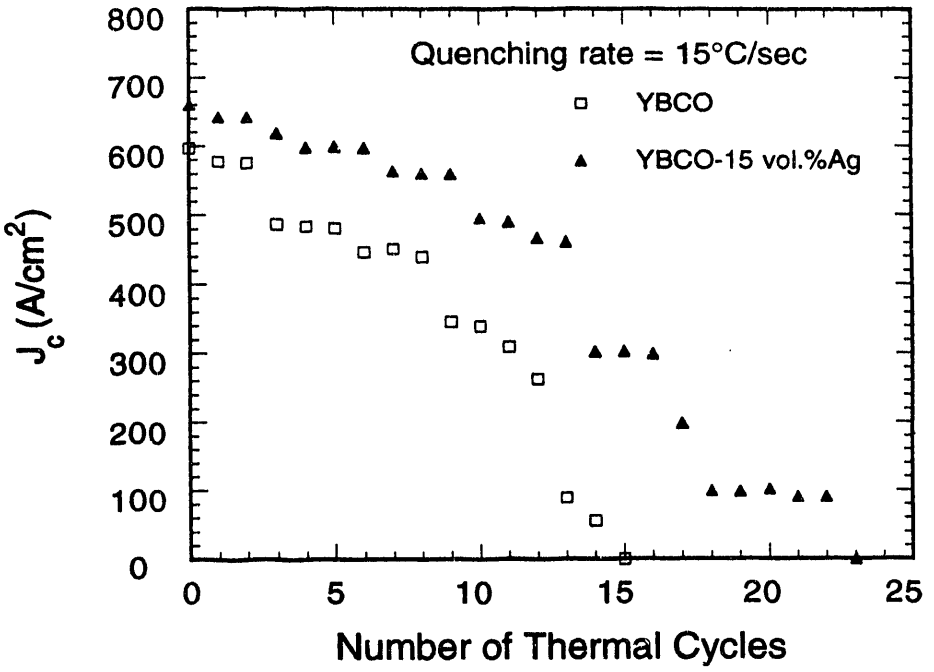

Fig. 11. Variation in J_c of YBCO wires versus number of quench cycles

related to the improvements in mechanical properties (strength and fracture toughness) of YBCO with Ag addition. The YBCO/Ag composites may have better resistance to initiation and propagation of microcracks.

The nature of delayed failure was studied by measuring strength σ_f of YBCO wires as a function of loading rate $\dot{\sigma}$ at room temperature and atmospheric conditions and evaluating the value of the subcritical crack growth parameter, N ($\sigma_f = A\dot{\sigma}^{1/(N+1)}$). To obtain different loading rates, the crosshead speed was varied from 0.0025 to 0.5 cm/s. The loading rate was determined from the slope of load-displacement curves, which indicated a range from ≈0.3 to 90 MPa/min.

Figure 12 shows the dependence of the strength of YBCO and YBCO/Ag wires on loading rate. From the slope of the straight-line fits, the values of subcritical crack growth parameter N were determined to be 35 for YBCO and 41 for YBCO/Ag wires. Although these numbers are comparable, a slightly higher value of N for YBCO/Ag composites indicates an improved resistance to subcritical crack growth. This slight improvement in resistance to subcritical crack growth of YBCO/Ag composites is believed to be due to induced compressive stresses in the YBCO matrix resulting from mismatch between the thermal expansion coefficients of YBCO and Ag (Kupperman et al., 1989). These compressive stresses may impede the growth of preexisting flaws. In addition, Ag particles may also deflect, bridge, and pin the propagating crack and minimize subcritical crack growth.

Effects of Ag additions on strain tolerance of Ag-sheathed PBSCCO tapes

Effects of Ag additions on microstructure, J_c, and strain tolerance of Ag-sheathed 2223 PBSCCO tapes have been evaluated. $Bi_{1.8}Pb_{0.4}Sr_2Ca_{2.2}Cu_3O_x$ tapes were made by powder-in-tube processing. Powders of both PBSCCO and PBSCCO/15–25 vol.% Ag composites were used to process the tapes. The process included packing Ag tubes with

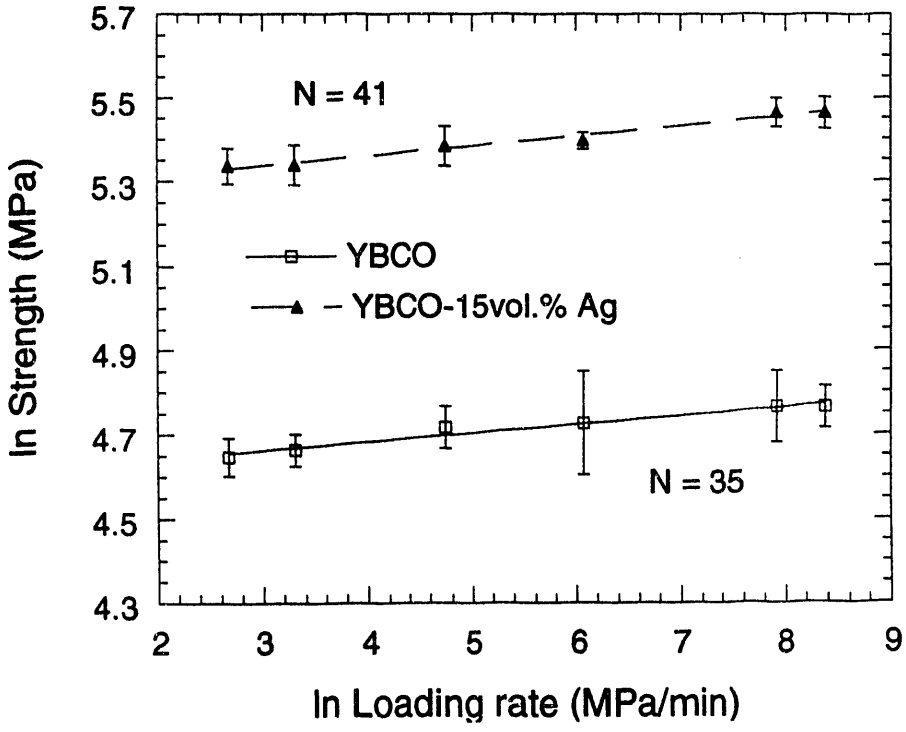

Fig. 12. Strength versus loading rate for YBCO and YBCO/Ag wires

superconducting powder (PBSCCO or PBSCCO/Ag), followed by swaging, drawing, and rolling the tube to form thin tapes. X-ray analysis of the tapes made from PBSCCO and PBSCCO/Ag powders sintered at 830–840°C for 50 h in 10% O_2 indicated that the degree of texturing increased with increasing sintering temperature and that the maximum 2223-phase content was obtained at 835°C. Maximum J_c values were atttained for the tapes made from both powders sintered at 835°C. Therefore, 835°C was selected as the optimal sintering temperature for further heat treatment. The tapes made from both powders were subjected to repeated heat-treatment cycles (sintering at 835°C for 50 h in 10% O_2) and mechanical pressing (≈1000 MPa) to introduce desired texturing of the PBSCCO grains. The BSCCO tapes subjected to six thermomechanical cycles resulted in the best J_c of 9600 A/cm^2 at 77 K and 124,000 A/cm^2 at 4 K in a zero applied field. The J_c values for the tapes made from BSCCO/15 vol.% Ag powder were 9900 A/cm^2 at 77 K and 120,000 A/cm^2 at 4.2 K. Higher volume fractions of Ag additions or additional thermomechanical treatment resulted in slightly decreased J_c values.

Selected sets of Ag-sheathed PBSCCO and PBSCCO/Ag tapes were subjected to a predetermined level of tensile strain (to 2.5%) in a uniaxial mode to evaluate the effects of Ag additions on strain tolerance, as measured by retained J_c after the application of strain. Figure 13 shows the value of retained J_c as a function of applied strain. The fraction of J_c retained after the application of strain was higher for the PBSCCO/Ag composite tapes than for the monolithic PBSCCO tapes. For example, for a 1.2% applied strain, 90% of initial J_c was retained for PBSCCO/15 vol.% Ag composite tapes, compared with only 40% retention for the monolithic PBSCCO tapes. Similar observations have been made by Miller et al. (1991). In these superconducting tapes, the application of strain causes the formation of cracks, which together with microcracks, reduce J_c. The addition of Ag increases the

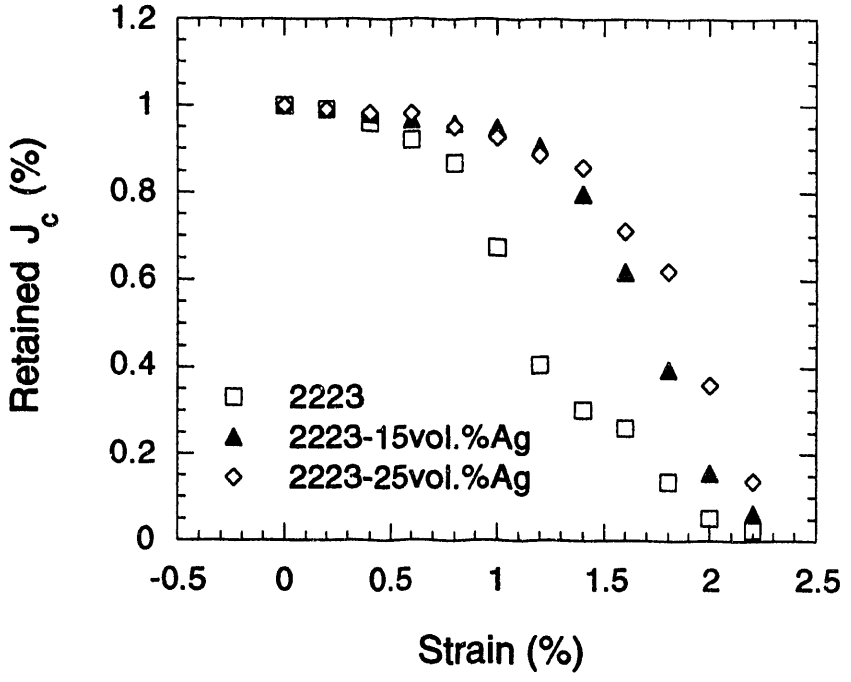

Fig. 13. J_c versus number of quench cycles for Ag-sheathed PBSCCO

fracture toughness of PBSCCO (Singh et al., 1993). The increased toughness provides higher resistance to crack formation and propagation, which, in turn, as a result of Ag additions, increases the retained J_c and strain tolerance of PBSCCO tape.

Figure 13 also shows the data for BSCCO/25 vol.% composites, which indicate an improvement in relative strain tolerance, but with decreased absolute values of J_c. Therefore, 15–20 vol.% Ag addition to PBSCCO is believed to be the composition that provides optimum mechanical and superconducting properties.

Monolithic 2212 BSCCO

The K_{IC}, strength, and hardness of fully dense monolithic BSCCO 2212 have been measured. The specimens were fabricated by hot isostatic pressing (HIPing) and sinter forging (Chu et al., 1992). The HIPed specimens exhibited moderate textures in which the c axes were aligned preferentially to the top and bottom faces. The sinter forgings exhibited much stronger textures. Fracture toughness was dependent on orientation, with the values ranging from 2.7 to 3.2 $MPa(m)^{0.5}$ for the HIPed specimens and 3.2 to 3.9 $MPa(m)^{0.5}$ for sinter-forged specimens. These values are higher than those obtained for YBCO. Delamination between grains, or between planes within grains, occurred during fracture. The average Vickers hardness for the specimens was 9×10^2 MPa, which is fairly low for a ceramic, and the strengths were less than ≈100 MPa, which is also very low.

High-temperature deformation

High-temperature mechanical-deformation studies were completed for YBCO. The relationship between creep and diffusion was demonstrated. Tracer-diffusion measurements indicated that Y diffuses with an activation energy of 1000 ± 200 kJ/mole (Chen

et al., 1992a), which agrees well with the value for creep of 970 ± 130 kJ/mole (Goretta et al., 1990b). This value is very high for a ceramic with such a low melting temperature and indicates the inherent difficulty in sintering YBCO.

Creep testing of 2212 BSCCO was completed. Diffusional flow occurred when the specimens were compressed at 780–835°C under low stresses. The activation energy for the deformation was 990 ± 190 kJ/mole, which is quite similar to that for YBCO. No effect of deformation on oxygen partial pressure was found (Routbort et al., 1992).

2.3.5 Nondestructive Evaluation

$Bi_{1.8}Pb_{0.4}Sr_2Ca_2Cu_3O_x$/Ag superconducting tapes

An ultrasonic technique to detect and monitor formation of the transient liquid phase during heat treatment of $Bi_{1.8}Pb_{0.4}Sr_2Ca_2Cu_3O_x$ (PBSCCO)/Ag superconducting tapes is being explored. It is believed that a liquid phase is essential in achieving proper phase development, grain alignment, and subsequent optimal superconducting properties (Kaufman et al., 1993; Poeppel et al., 1993). The end of the sintering cycle should be determined by the disappearance of the liquid. At present, there is no information about when during sintering the liquid phase forms and when it disappears. An ultrasonic technique is being evaluated to measure the velocity of sound in the tape, which may be sensitive to the amount of liquid present. In addition to the ultrasonic experiments, some of which have already been completed, we will carry out experiments at the ANL Intense Pulsed Neutron Source (IPNS) to validate the ultrasonic technique.

PBSCCO/Ag tapes, about 250 μm thick, 4 mm wide, and 3 cm long, were prepared at ANL by the powder-in-tube method (Kaufman et al., 1993). The tapes were sintered in air at 845°C, while the velocity of sound was monitored to detect the appearance and disappearance of liquid phase in the PBSCCO. A magnetostrictive transducer launched a 140-kHz wave in a 2-mm-diameter remendur rod, which was welded to an Inconel rod, which in turn was attached to the superconductor by either a ceramic cement or electron-beam welding. Clear echoes were evident from the tape/rod interface and from the ends of the tape. The round-trip transit time of the tape, which was entirely inside the heated furnace, was monitored. The transit time increased with temperature as the tape expanded and the material composite elastic modulus decreased. A reference experiment was carried out in which the temperature of the tape was increased continually at a fixed rate (Fig. 14). Curves obtained by DTA indicated that incongruent melting occurred in air at 840–870°C. As the temperature of the tape rose, there was a relatively rapid increase in transit time (Δt) over the temperature range in which a liquid was expected to form. This rise in Δt implies that the velocity dropped, as expected, when the low-sonic-velocity liquid was mixed with the higher-velocity Ag and solid PBSCCO. This result suggests that velocity measurements can be used to determine the presence of liquid.

Figure 15 shows an example of the round-trip transit time of an ultrasonic wave as a function of the temperature of a PBSCCO/Ag tape that was monitored during sintering, when the transit time rose and then fell as the tape was held at 845°C. This rise and fall could be the result of the appearance and gradual disappearance of liquid, suggesting that the decrease in liquid phase can be followed by monitoring the velocity of sound. In this example, SEM images prepared after the test indicated that melting did, in fact, occur in the tape.

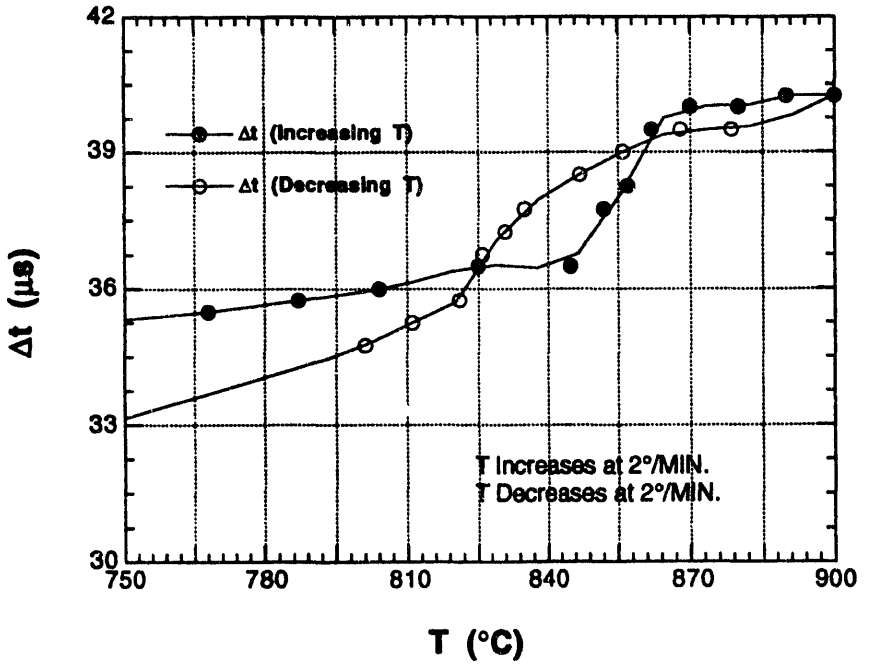

Fig. 14. Round-trip transit time of longitudinal ultrasonic wave as a function of temperature in PBSCCO/Ag tape for steadily increasing and decreasing temperatures. Rise in Δt at ≈840-870°C on heating is attributed to incongruent melting; upon cooling, decrease is attributed to temperature-dependent changes in mechanical properties.

To validate the ultrasonic method of monitoring the liquid phase in PBSCCO/Ag, tapes will be examined by neutron scattering. Because the velocity of sound can be influenced by variations in porosity and neutron results would not, the neutron experiment will help establish the sensitivity of the sound-velocity technique to detect the formation of liquid. The IPNS at ANL provides a white spectrum from which we believe the appearance of an amorphous component in the sintering of a PBSCCO/Ag composite can be detected. Subtle changes in the microstructure of the BSCCO/Ag can be observed by comparing peak heights in the neutron-diffraction spectrum and by a general increase in background. We will look for slowly oscillating variations in the background of the neutron-scattering spectra caused by liquid material. Some reference data are already available, as past IPNS BSCCO experiments focused on phase development of BSCCO powders. X-rays will not be useful because of the Ag sheath. Samples prepared for XRD are open-faced, and Pb and Bi volatility would be a problem.

Correlation of levitating force with texture

ANL and Allied-Signal, Inc., are engaged in a program to understand the factors that affect the levitation properties of YBCO and to improve the quality control and evaluation techniques for YBCO, a candidate material for high-T_c superconducting magnetic bearings. The levitating force of a YBCO sample should correlate strongly with the alignment of the c axes, although simply aligning the grains should not result in a significant increase in the

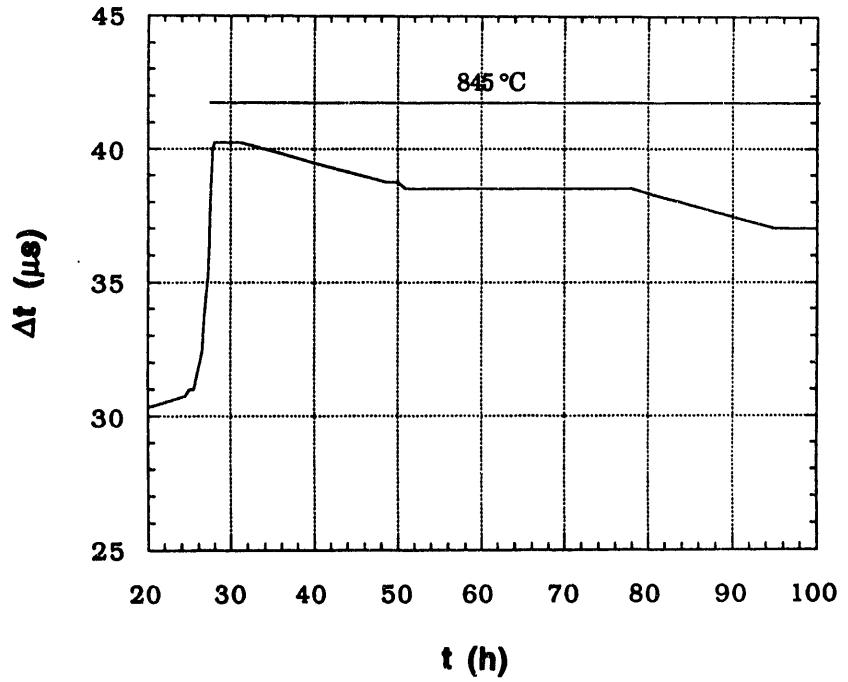

Fig. 15. Transit time of longitudinal ultrasonic wave in PBSCCO/Ag tape as a function of time; temperature rises to 845°C at ≈28 h and is then held constant

levitation force unless there is a concurrent increase in pinning. Critical currents increase significantly with grain size and pinning, independent of orientation (Jin and Graebner, 1991). It would be useful to assess, through bulk measurement, whether texture (c axis normal to surface) alone correlates strongly with levitation force. Neutron diffraction analysis can be used to determine the bulk texture and to validate the ultrasonic results (Biondo et al., 1992). In addition, it may be possible to map the texture spatially by mapping the ultrasonic velocity of sound, a method that must be validated but, if viable, will provide the simplest and quickest method to map texture (and possibly levitating force) of a sample at room temperature. Simultaneously, an ultrasonic scan could provide the control necessary to assure a high-quality product by detecting undesirable cracking and porosity in mass-produced bearings. An ultrasonic technique could be easily adapted to a production line environment with minimum safety hazards while still providing a simple, effective system for assessing process control and quality.

Neutron diffraction and ultrasonic velocity-of-sound mapping techniques have been used to quantify the relationship between texture and levitating forces of various samples produced by different techniques at Allied-Signal and ANL. Neutron diffraction analysis (at the IPNS and the University of Missouri Research Reactor) has been used to quantify bulk texture. Figure 16 shows the texture represented as a ratio of the {004} to the {100} diffraction line intensities as a function of levitating force. There is a strong correlation. Figure 17 shows the velocity of sound for normal incident longitudinal waves as a function of levitating force. These two figures indicate that texture may be used to predict levitating force and that the velocity of sound measurement is sufficiently sensitive to indicate, at room temperature, what the relative magnitude of the levitating force will be for comparable samples at cryogenic temperatures. In addition, it is possible to map texture

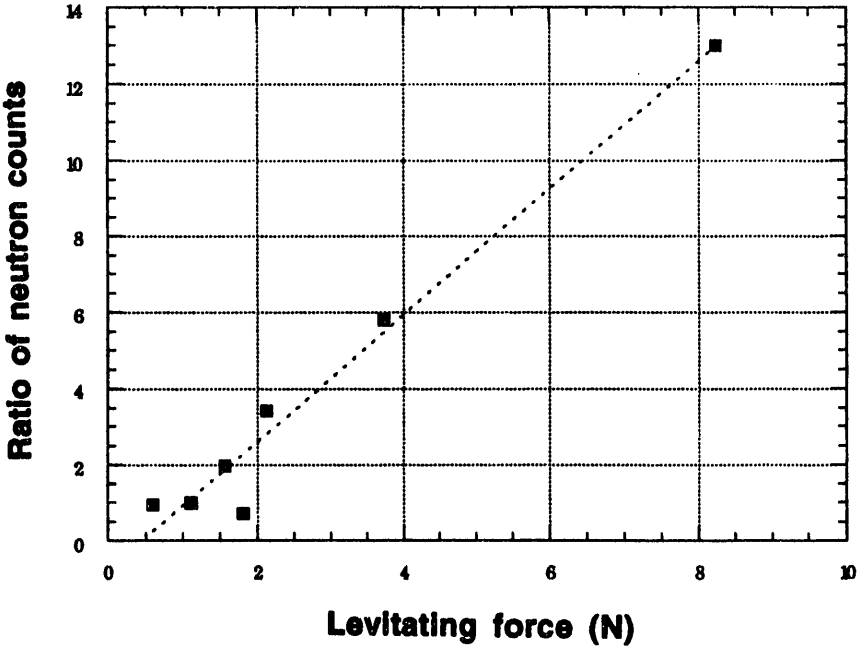

Fig. 16. Ratio of neutron counts for c-axis (004) and a-b plane (100) lines versus levitating force

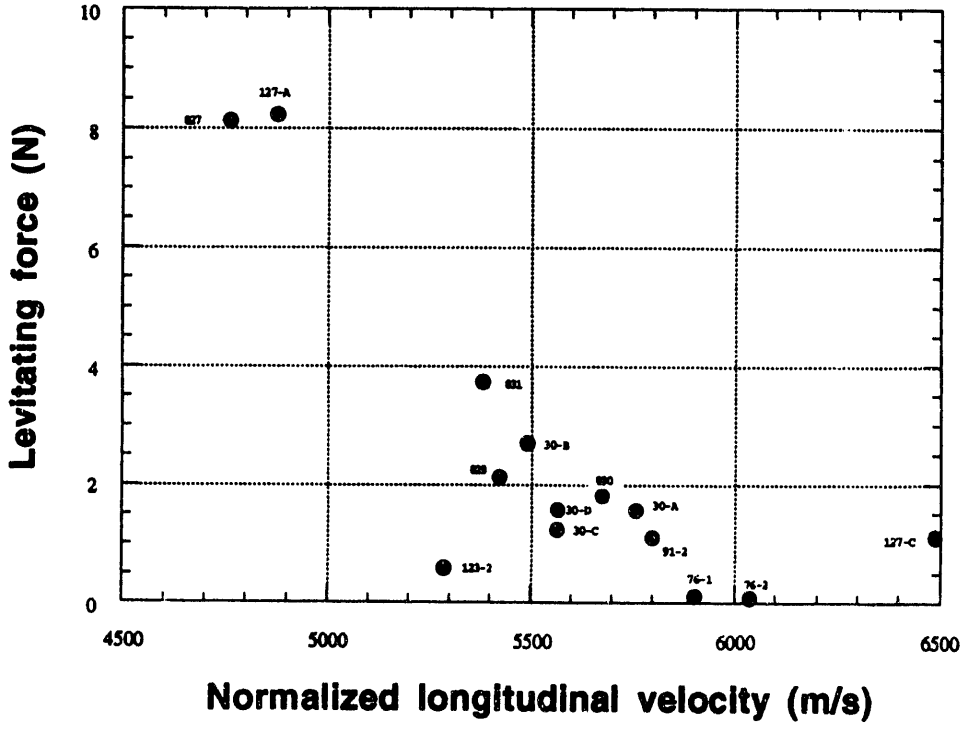

Fig. 17. Levitating force as a function of normal incident longitudinal velocity of sound; velocity values are normalized for variations in density

spatially by mapping the ultrasonic velocity of sound (which could be validated by neutron diffraction). Because the dependence of shear wave velocity on crystallographic direction is too complicated to be useful and values of elastic constants for shear waves are not well defined, only longitudinal waves have been employed. In addition to conventional high-frequency experiments carried out at ANL, an ultrasonic dry-coupling scanning system, developed at NASA Lewis Research Center, has been used to map longitudinal velocity of sound in a YBCO disk. Conventional scanning systems require a liquid couplant, which could damage the YBCO samples.

We have shown that the longitudinal velocity of sound can be used to detect and help understand texture-induced anomalous magnetic-field patterns. In the experiments discussed here, the levitating force varied from 0.1 to 9 N. There was a clear indication of preferred orientation, as provided by neutron diffraction data for samples with very high levitating forces (and low velocity), and little texture was indicated for samples with low levitating force (and high velocity). The average longitudinal velocity of sound varied from 4100 to 5600 m/s when a through-transmission ultrasonic technique, employing a 13-mm-diameter transducer, was used. Other factors, such as grain size, may play a role sufficiently important to prevent a strong correlation between velocity and levitating force.

For an ultrasonic scan of a YBCO disk carried out at NASA-Lewis Research Center, the analysis of the data indicated spatially varying velocity (1-mm resolution), with a range of 4000-6000 m/s. Because the velocity of fully dense material, based on elastic constant data found in the literature, can vary from 4600 to 5900 m/s, depending on propagation direction, the results from NASA are considered reasonable. The lower velocity measured could be the result of less-than-theoretical density in some areas of the disk. A gray-scale velocity map showing "ultrasonic structure" comparable to the observed grain structure was provided.

2.4 Applications and Devices

2.4.1 Current Leads

Current leads employed for the transfer of electrical energy from ambient-temperature devices to cryogenic-temperature devices (Wu et al., 1991) afford an area for the viable near-term application of high-T_c superconductors. High-T_c superconductor current leads offer the advantage of reduced low-temperature refrigeration loads because they eliminate Joule heating and reduce thermal conduction along the lead. Suitable bulk high-T_c superconductor materials are available with current densities at 77 K of 100-1000 A/cm^2, which results in thermally efficient, reasonably compact, current-lead assemblies at acceptable cost. Details of a generic high-T_c superconductor current lead are shown in Fig. 18.

Near-term applications include superconducting magnets for particle accelerators, storage of magnetic energy, superconducting motors, and space-based cryogenic devices. The objective of our development program is near-term commercialization of high-T_c superconductor current leads. The program includes development of conductors, analysis of performance, design and fabrication of leads, and evaluation of lead performance.

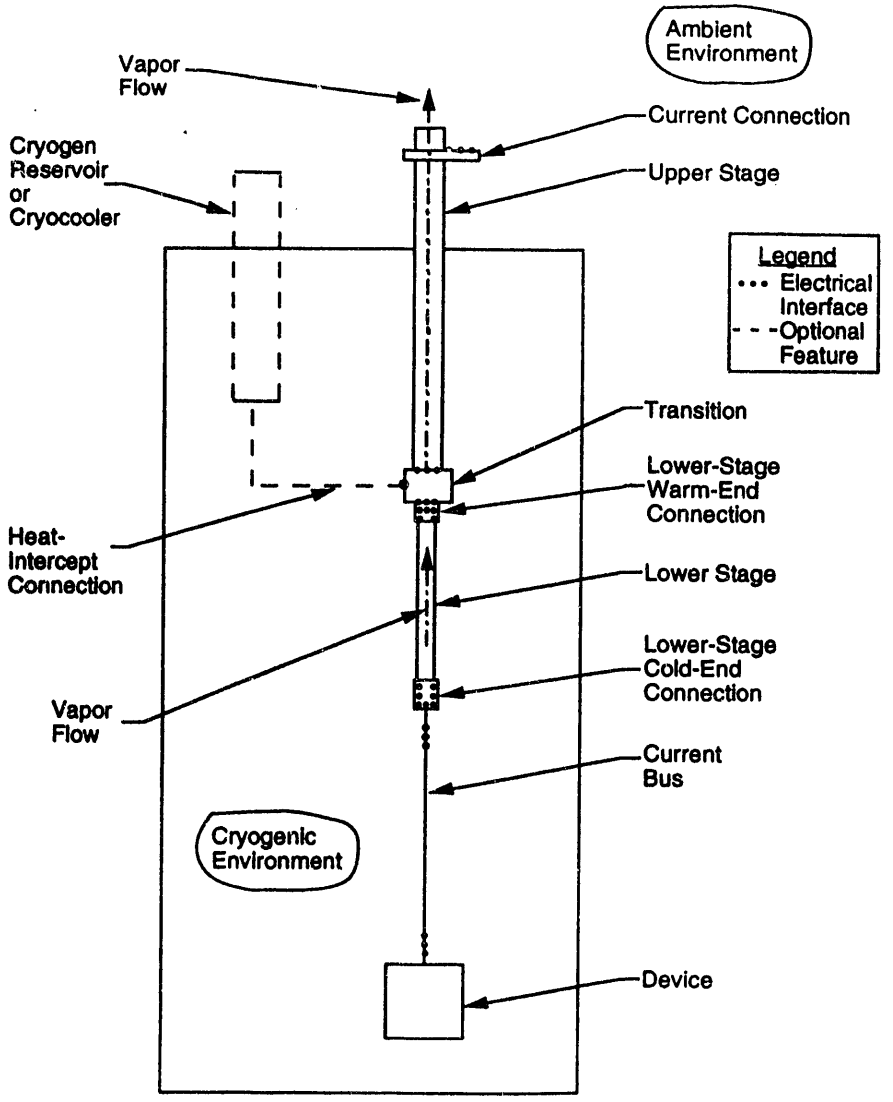

Fig. 18. Schematic diagram of current lead

The conductor development program considers critical-current characteristics, AC losses, mechanical strength, fracture toughness, thermal shock and cycling, and ceramic-conductor-to-metal transition. Typical properties for YBCO with 15 vol.% Ag in bulk rod form are J_c = 100–200 A/cm^2 at 77 K and 15 mT, flexural strength = 180 MPa, and K_{IC} = 3.2 MPa(m)$^{1/2}$ (Singh et al., 1989). Ag/ceramic interfacial area specific resistances of 10^{-7} W-cm^2 are achievable.

Performance analysis considers conductor material, operating modes, and operating conditions. The analysis treats the entire lead assembly under both steady-state and transient conditions. Predicted thermal performance (i.e., heat leak) of a 300–4 K current lead employing a YBCO/Ag conductor is 0.8 mW/A for self-cooling, and 0.1 mW/A lead with a 77 K intercept. For comparison, the corresponding value for a conventional lead, e.g., vapor-cooled copper, is 1 mW/A for self-cooling.

Component design and fabrication considers lead performance, reliability, safety, manufacturability, and cost. A 100–A capacity lead has been designed and fabricated, and is undergoing performance evaluations. The lead incorporates a conventional upper stage, a transition suitable for heat interception, and a lower stage that incorporates a YBCO/Ag conductor. Designs are proceeding on larger capacity, I > 1000 A, leads suitable for installation in commercial cryogenic devices. Prototype lead assemblies will be fabricated and evaluated under typical operating conditions.

Performance evaluation experimentally considers the performance of high–T_c superconductor leads in the areas of critical current, heat input, voltage drop, pressure drop, connection resistance, and transient response. A current–lead heat–leak measurement facility has been designed, constructed, and is in operation. The facility is sized to accommodate 100–A leads. The measurement dewar is shown schematically in Fig. 19. The facility has measured the performance of conventional and high–T_c superconductor leads operating between 300 and 4 K. The agreement between measured and predicted performance was good. Measurements continue with leads of different design and operating mode.

2.4.2 Cryostabilization of High-Temperature Superconducting Magnets

A new concept for stabilizing magnets made from high–T_c superconductors was developed (Cha et al., 1992). A critical issue yet to be resolved in determining the ultimate commercial viability of high–T_c superconductors at liquid N_2 temperature is protection of the magnet during a quench. The specific heat of the stabilizer (most likely Ag) is rather high at 77 K, and the propagation velocity of a normal zone is extremely low. Consequently, protection of a medium or large high–T_c superconductor magnet operating at liquid–N_2 temperature by the conventional technique of self–propagation is not likely and presents a challenge to magnet designers.

We have proposed and analyzed the possibility of providing full cryogenic stabilization of high–T_c superconductor magnets by flowing subcooled liquid N_2 through microchannels. Microchannel cooling is an emerging technology that has been used in electronic packaging and microminiature refrigeration devices. The maximum possible heat removal rate in this type of heat transfer is much larger than that for pool boiling. The results of our analysis demonstrate that the use of subcooled liquid N_2 flowing in microchannels can successfully cryostabilize high–T_c superconductor magnets. The achievable current densities are comparable to the best values attained in contemporary superconducting magnets. High stability is attained at the cost of a significant, but not inordinate, pressure drop in the cooling channels. This pressure drop can be readily accommodated by flowing the coolant transversely to the current flow. In addition to pressure drop, coolant temperature rise and fin–tip temperature were also identified as primary design constraints for a microchannel system.

Compared with a conventional superconducting magnet, magnets used under microchannel–cooling conditions will require significantly more manifolds. To keep system pressure drops practical, it will be necessary to establish short flow paths, and we have suggested running flow perpendicular to the current. For a pancake magnet formed by tape conductors, there is a good match between conductor width and length of coolant flow. An

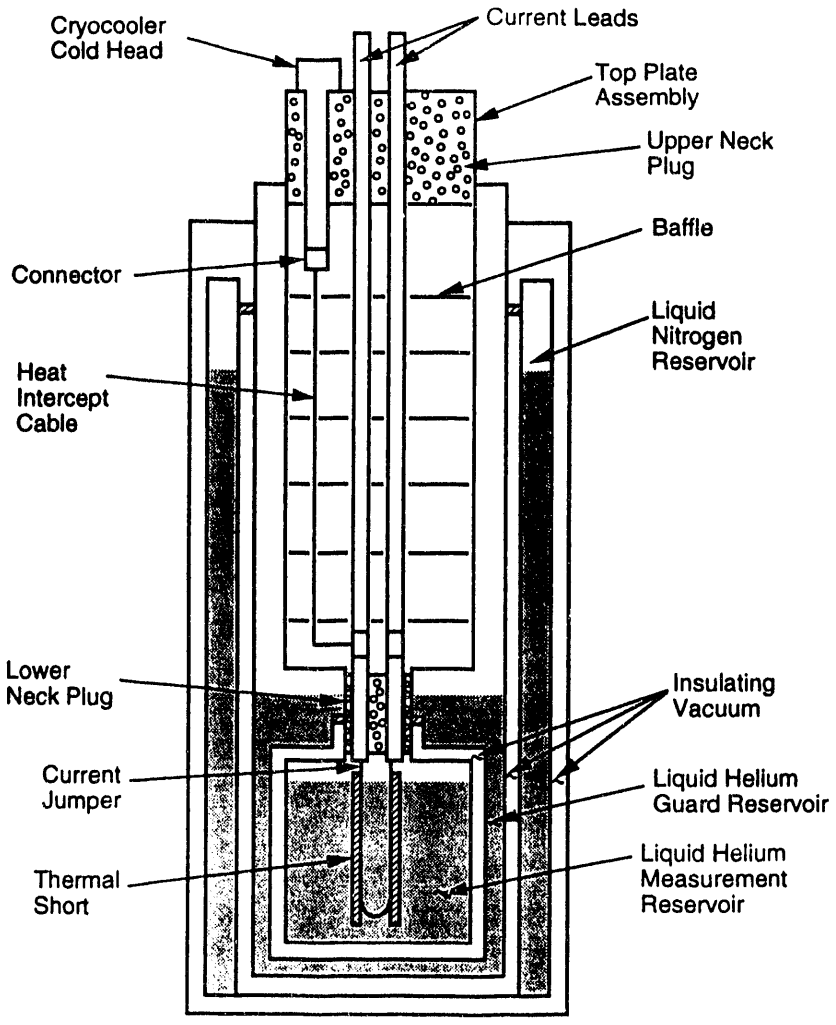

Fig. 19. Dewar assembly for testing current leads

alternate configuration would be to run the coolant flow in the direction of the current, but have periodic flow inlets and outlets. Such an arrangement could complicate the winding of a large magnet.

Fabrication of microchannels in conductor stabilizers may require more precision than is typical in the fabrication of conventional superconductors. The channels could be etched onto the stabilizer after final conductor processing or could be manufactured on a separate piece and postbonded to the stabilizer (Hull et al., 1992). Clearly, the fabrication costs of the microchannels must not be excessive if the stabilization technique is to be viable. The microchannel approach described here is readily adapted to operation at temperatures lower than 77 K. Pure liquid N_2 can be subcooled considerably below the boiling point, with the minimum temperature depending on pressure. A mixture of N_2 and a small amount of Ne could lower the freezing point of the cryogen even further.

2.4.3 Superconducting Magnetic Bearings

The effort to develop improved magnetic bearings (Weinberger et al., 1991) that are based on the levitation properties of YBCO superconductors has continued. The flux-pinning characteristics of superconductors allow stable levitation of a rotating bearing without the position sensors and elaborate feedback control systems that are required to achieve stability with conventional active electromagnetic bearings. It is not necessary to achieve high current transport between the grains of a superconductor to achieve good levitation characteristics, and the inter-granular magnetization properties of melt-textured YBCO materials are adequate for many bearing applications that involve rotating electrical machinery and energy-storage flywheels.

During FY 1991 and 1992, technical breakthroughs occurred that enable extremely low rotational losses with high-T_c superconducting magnetic thrust bearings. In a collaborative effort with the United Technologies Research Center, bearing coefficients of friction (defined as rotational drag-to-lift force ratio) as low as 3×10^{-6} have been measured wuth small rare-earth permanent-magnet rotors and YBCO stators. In contrast, conventional mechanical bearings and active magnetic bearings have coefficients of friction in the range of 10^{-2}–10^{-4}. Use of high-T_c superconductor magnetic bearings should enable the development of high-specific-energy flywheels with rotational energy losses in the 0.1%/h range, as contrasted to losses of 1%/h or more for conventional flywheels. Consequently, high-T_c superconductor bearings are an enabling technology for flywheels used in diurnal energy-storage applications.

An apparatus for testing superconducting bearings was assembled during FY 1992. The apparatus includes a high-capacity diffusion vacuum pump, auxiliary pumps, an ionization vacuum gauge/controller, a liquid N_2 cooling system, and a 30-cm-diameter bell jar test section. The test section (illustrated schematically in Fig. 20) includes a liquid N_2 cold chamber for cooling YBCO stator elements, positioning devices for proper placement of permanent-magnet/flywheel rotor assemblies, mechanisms for flywheel rotor spinup, and a photocell detector to measure spindown history. Spinup tests were accomplished with either a dry-N_2 gas jet or a retractable induction motor assembly.

A 9-cm ring magnet was successfully used to levitate and rotate a 600-g flywheel assembly. This assembly consisted of the ring magnet attached to the bottom of a 10-cm-diameter aluminum flywheel, with an small steel rotor mounted on top for use during induction-motor spinup. Other efforts during FY 1992 involved characterization and enhancement of rare-earth permanent magnets for high-T_c superconductor bearing applications. The azimuthal inhomogeneities in the field of permanent-magnet rotors are known to be responsible for most of the electromagnetic losses associated with high-T_c superconductor bearings. Azimuthal field variations of commercially available disk and ring magnets are ≈5%, and can be improved by superimposing different magnets in layers and using ferromagnetic shims. The near-term goal is to develop a 500 W-h prototype flywheel that contains high-T_c superconductor magnetic bearings with energy dissipation <0.1%/h. Discussions have been held with several electric utilities that have indicated a strong interest in high-T_c superconductor bearing/flywheel technology.

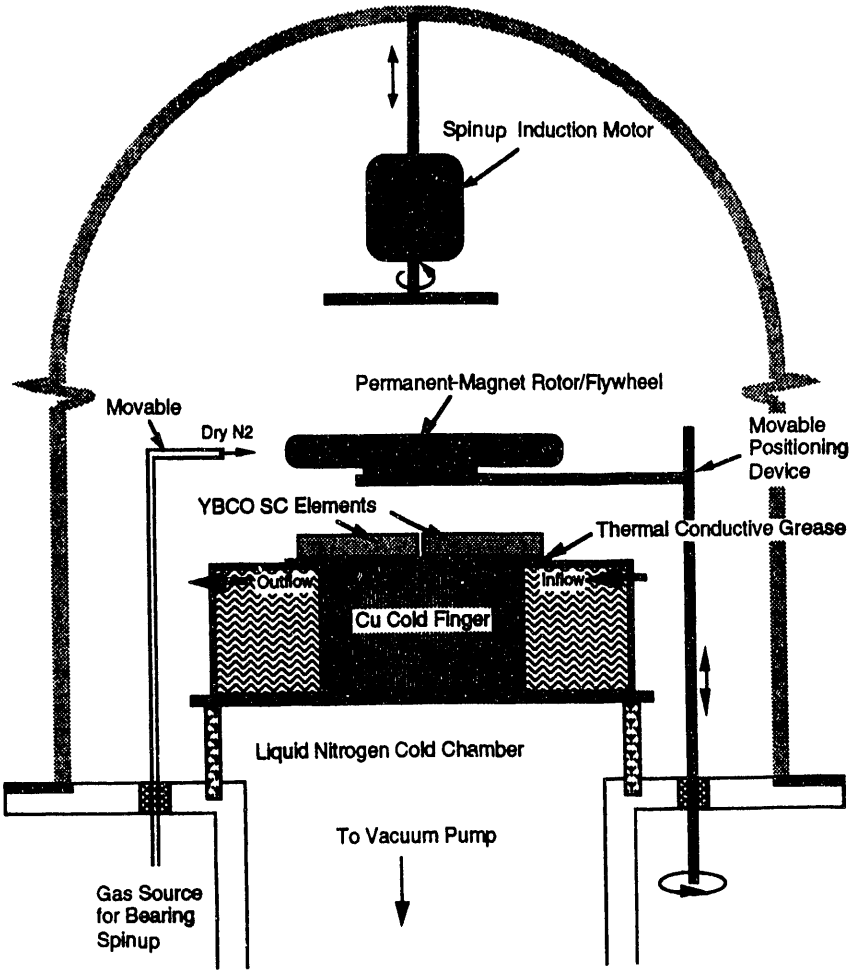

Fig. 20. Schematic diagram of apparatus for testing superconducting bearings

2.5 Microstructure and Transport Studies Relevant to Development of Practical Conductors

2.5.1 Technical Progress

One of the major accomplishments of this program has been to elucidate the irreversibility of the highly anisotropic high-T_c superconductors by considering the model of intrinsic Josephson coupling between neighboring Cu-O bilayers (Kim et al., 1991). With this model, we predicted that TBCCO 1223 is currently the best alternative to YBCO for operation at high magnetic fields and temperatures. This has been adequately verified and a significant research effort has begun worldwide. We are developing materials and techniques for processing TBCCO 1223 and other candidate materials. A crucial link between superconducting transport properties and the preparation conditions is forged through state-of-the-art microstructural characterization.

Another issue is to determine the ultimate potential for current-carrying capacity in the high-T_c superconductor materials, in terms of both optimized flux pinning within grains and intergranular coupling. For flux pinning, we eliminate grain boundaries by

studying epitaxial deposits and single crystals. In addition, specific grain boundaries are isolated, e.g., between epitaxial deposits. Microstructural visualization plays an important role here too, i.e., to determine the existence and characteristics of pinning defects, grain boundaries, and other weak links.

Materials development: reduced anisotropy

The most optimistic current transport results for a polycrystalline material were reported by General Electric Corporation (GE) for materials grown in a thick-film geometry (Tkaczyk et al., 1992). As part of our collaboration with GE, we performed transport measurements in an applied magnetic field. These measurements indicate that, although the critical currents are large in these samples, they are still limited by weak-link grain boundaries (Hettinger et al., 1992).

To determine the ultimate current-carrying capability of single-layer TBCCO compounds, we successfully made $TlBa_2CaCu_2O_x$ (Tl-1212) films, for which grain-boundary effects are absent. The transport critical currents for several materials, both epitaxial and polycrystalline, are shown in Fig. 21; all were measured at the same value of reduced temperature (T/T_c). The low-field behavior of the Tl-1212 films is comparable to that of the Tl-2212 epitaxial films, whereas the irreversibility line, where the critical currents cut sharply to zero, coincides with Tl-1223 thick films deposited at GE. We also measured the resistive transitions of phase-pure Tl-1223 and nearly phase-pure Tl-1212. The results fit well into the proposed framework when reasonable parameters describing the superconductivity were used. The irreversibility lines of these materials were far superior to double-layer compounds containing either Bi or Tl, in agreement with the concepts put forth by our model (Kim et al., 1991).

Effects of grain boundaries and flux pinning on current-carrying capacity

Extrinsic defects such as grain boundaries are well known to be detrimental to the dissipationless current-carrying capacity of high-T_c superconductors. It is important to gain an understanding of the mechanisms that lead to the observed dissipation. This will allow at least a prediction of the electric field/current density (E-J) characteristic in polycrystalline materials to levels below the measurable limit and, then, an extrapolation to the practical lengths of material needed in high-magnetic-field devices.

YBCO containing a series of (001)-tilt grain boundaries has been characterized microstructurally (Luine et al., 1992) and by electrical transport (Hettinger et al., 1992). From the broadened resistive transition at fields smaller than 10^{-2} T, and from the shapes of E-J curves of the sample measured, we have concluded that the grain boundaries behaved as weak links. These curves were similar to those generated from the Ambegaokar-Halperin model (Ambegaokar and Halperin, 1969), which is valid for a single Josephson junction (JJ) where fluctuations of the phase across the JJ are important. Fitting this model to our data yielded activation energies that may be compared to activation energies extracted from the resistive transitions. The agreement of these quantities was excellent (Hettinger et al., 1992). The conclusion from this result is that, regardless of the coupling energy, there always exists an ohmic region of the E-J curve at small current densities; however, it occurs at smaller dissipations as the coupling energy is increased.

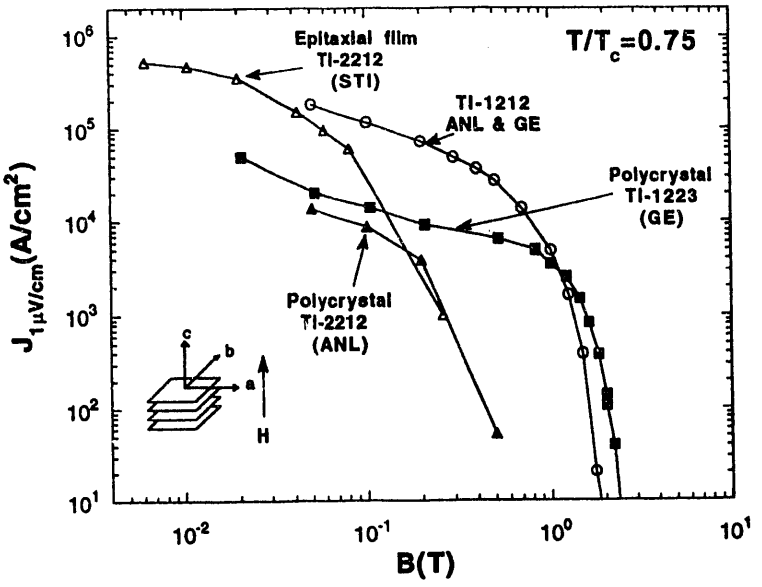

Fig. 21.
J_c versus field for several TBCCO samples measured at ANL

Measurements on polycrystalline and epitaxial Tl-2212 films showed similar behavior at low current density; however, the resulting dissipations diverged at higher current density. The polycrystalline material had a J_c one order of magnitude lower than that of an epitaxial film. The curvature of the E–J characteristic was very different and may be attributed to the Ambegaokar-Halperin behavior discussed above. At low currents, the dissipation was dominated by the intragranular behavior, unlike the dissipation of the YBCO tilt-boundary sample.

Further measurements on epitaxial materials have indicated that there is a change in the shape of the E–J characteristic at the dimensional crossover of the vortices. If this dimensional crossover is the practical definition of the useful limit of these materials for high-field/high-current applications, we must find more effective ways of pinning the vortices in two dimensions. Recently, work performed at Oak Ridge National Laboratory on ion irradiation of highly anisotropic BSCCO 2212 (Thompson et al., 1992) has been evaluated by our group (Kim et al., 1992). Our analysis of this work shows that pinning can be increased in a system of two-dimensional vortices if a defect is introduced in each and every Cu-O plane, as is accomplished when columnar defects are used. Ion irradiation is not practical for large-scale applications, but defects of the required geometry might be introduced by other means.

The effect of mechanical deformation (Routbort et al., 1992) and HIPing (Goretta et al., 1992c) on the development of microstructure has been studied for BSCCO 2212 to gain insight into the thermomechanical processing steps required for fabrication of wires and tapes. The microstructure evolves from a loose packing of powders to a fully dense structure within 15 min of HIPing at 825°C. Samples deformed at high temperature under compression have shown that strain is accommodated by a combination of dislocation glide and microcracking. Transmission electron microscopy confirmed that densification during HIPing occurs by those mechanisms and yields a high density of dislocations within the grains. Further HIP time results in the annihilation of these defects by recovery processes, including the formation of subgrain boundaries.

Transport measurements showed low intergranular critical currents for all samples, indicating weakly coupled grain boundaries, whereas samples HIPed short times showed enhanced magnetic hysteresis compared to those HIPed longer times, suggesting improved intragranular critical currents. A sample subjected to controlled deformation by creep exhibited an even more significant enhancement in magnetic hysteresis (Miller et al., 1992). The microstructural basis for this behavior is the high dislocation density produced in samples subjected to deformation. These defects serve as flux-pinning centers and result in improved intragranular currents. The critical current estimated from the magnetization data has also been compared to transport data from a single crystal and found to be in good agreement, establishing a critical link between those types of measurements (Miller et al., 1992). These techniques may be applied to current transport through textured "brickwork" samples.

2.5.2 Status

Low-anisotropy materials

One of our main objectives is to make films of Tl-1223 with improved microstructures and current-transport properties. This will be attempted by increasing the reaction temperature, varying the precursor composition, specifically the Tl, and increasing precursor density by sputtering. We will investigate the microstructural differences of films grown from Tl-free precursors and precursors containing Tl. Should denser precursors prove advantageous, we will explore methods for fabricating them on a continuous basis with Ag-buffered flexible metal substrates. We also hope to achieve epitaxial Tl-1223 films to determine the ultimate current-carrying capability of this compound.

Our work in developing processing techniques for Tl-1223 will proceed in two areas. We will continue our studies of the development of texture and phase evolution during the thermomechanical processing of Tl-1223 wires and tapes (Goretta et al., 1992). The effect of intermediate mechanical work and annealing sequences will be evaluated in terms of the impact on phase assemblage and microstructure, and will be related to our results from the BSCCO system. In addition, the effects of surface treatment of the sheath material will also be investigated. To aid processing of Tl-1223 by any method, the phase diagram in the Tl-Ba-Ca-Cu-O system will be investigated. Initial studies will concentrate on the mechanisms of Tl incorporation into thick films; they will then be expanded to identify the stability regions of the 1223 phase.

Reduced anisotropy is clearly important to raising the H-T irreversibility line and thereby improving conductor performance. We will examine a new class of compounds, based on $(Ca,Sr)CuO_2$, where the two dimensional CuO_2 layers are separated only by Ca(Sr) metal ions. These so-called infinite-layer superconductors should be the least anisotropic of all the high-T_c superconducting compounds, with reported superconductivity onsets as high as 150-170 K.

Grain boundaries and pinning

Single-grain-boundary studies of several materials are planned. TRW will provide single-step-edge samples for transport studies across grain boundaries. Westinghouse will provide a sample grown on a bicrystalline substrate for similar measurements. As our

fabrication program develops, we will grow a series of Tl-containing materials on bicrystalline substrates. A systematic, high-magnetic-field, large-current-density investigation of well-defined single-grain boundaries has yet to be performed.

The effects of columnar defects on pinning will be investigated in Tl-containing superconductors that are free of weak links. Defects may be introduced at ANL by ions of several masses, thereby creating defects of various sizes. This will allow an optimization of the size of defects needed for effective pinning, and it will place an upper limit on the practical critical currents attainable with these materials.

2.6 Additional Interactions

The objective of a program with Illinois Superconductor Corporation of Evanston, IL, was to improve the fracture resistance of YBCO wires that are to be used for currently produced and sold cryogenic-liquid level sensors. Several successful solutions were found, some of which could be adapted to the long, thin, superconducting wire made by Illinois Superconductor.

Addition of 15–20 vol.% Ag particles to YBCO doubled its fracture toughness K_{IC} and improved its strength. Improvements were due to the ductility of the Ag and favorable residual stresses; the brittle YBCO was in compression and the ductile Ag was in tension (Singh et al., 1989; Kupperman et al., 1989). Addition of Y_2BaCuO_5-coated ZrO_2 particles was also found to improve K_{IC}, possibly because of transformation toughening. Bars coated with 20 mol% ZrO_2 had a K_{IC} of 4.5 ± 0.4 MPa(m)$^{1/2}$, but because of porous regions near some of the ZrO_2 additions, had low strength (Goretta et al., 1991). It was thought that the control of microstructure by sintering at lower temperatures and lower oxygen partial pressures, would produce a fine-grained superconductor with higher strengths. This technique has shown promise and fracture strengths of 230 MPa have been obtained (Chen et al., 1992b).

Glazing proved to be the least expensive, most efficient technique for improving the strength and reliability of the wires. A low-melting-temperature glass was dispersed in a liquid into which the wires were dipped. The wires were then dried and fired. The resultant composite maintained its superconducting properties and had a load-to-fracture 3–5 times that of unglazed wires. The enhancement depended on the type and thickness of the glass. The T_c of the wires remained unchanged. A senior engineer from Illinois Superconductor spent a week at ANL learning and applying the technique.

The collaboration between IBM (Yorktown Heights, NY) and the Materials Science Division of ANL has continued. Experiments have explored improvements in flux pinning of YBCO achieved by irradiation with different particles (Civale et al., 1990, 1991; Kirk, 1991). The most recent studies of high-T_c superconductors irradiated with high-energy heavy ions have indicated that a defect structure is produced that is extremely effective in pinning magnetic flux lines. In attempting to develop models to account for these observations, it is imperative to have a complete characterization of the defects responsible for the property enhancements. Analyses by TEM of the microstructures of three single crystals of YBCO irradiated with different high-energy heavy ions show dramatically different damage characters. For Sn and Au projectiles with total energies of 580 MeV and 1.0 GeV, respectively, highly aligned tracks that extend many μm into the crystals were observed. Irradiation with 1.4 GeV Br ions, however, results in the formation of discrete

extended defects throughout the entire thickness of the crystal (≈30 μm). The nature of the defect tracks can be shown to depend qualitatively on the electronic energy loss S_e, of the incident ion as it slows down in the YBCO crystal.

In Fig. 22a, columnar tracks, induced in YBCO by irradiation with 580 MeV Sn ions, appear as discontinuous regions of amorphous damage along the length of the incident-ion path. This defect structure has been shown to produce extremely effective flux pinning at high temperatures and applied fields when the field is aligned with the tracks. Such a defect morphology may not be as effective in more anisotropic systems such as the Bi- and Tl-based superconductors (Kim et al., 1991). In these systems, a more continuous track is required to pin individual flux vortices along their entire length. Irradiation with 1.1 GeV Au ions produces such a defect track, as illustrated in Fig. 22b. The primary difference between the two cases is in the slowing rate of the ions, where S_e is 2.8 and 3.8 keV/Å for Sn and Au ions, respectively. This information also provides guidance for future irradiations aimed at studying flux pinning behavior.

The collaboration between Superconducting Products Company (Batavia, IL) and ANL has involved fabrication of Ag-clad wires. The Sr-deficient 2212 BSCCO powder synthesized at ANL (Bloom et al., 1991) was packed into Ag tubes and subsequently drawn to a diameter of ≈1 mm. Specimens were subjected to various thermomechanical treatments. Processing parameters that were controlled included the amount of reduction by rolling, and firing conditions, such as temperature, hold time, and atmosphere. To date, more than 100 separate sets of processing conditions have been tested, and the most significant parameter was found to be processing temperature. J_c values of ≈4 x 10^4 and 10^4 A/cm^2 at 4.2 K, measured from end to end, were obtained for a 1-cm-long tape and 1-m-long coil, respectively. The J_c did not change measurably in fields up to 50 mT or during a thermal cycle between room temperature and 4.2 K. Current work is focused on forming of tapes from Ag sheets so that the muzzle loading of tube working, and its inherent length limitations, can be avoided.

In the area of powder synthesis, calcination, and characterization, we continue to work with two companies: SSC, Inc. (Bothell, WA) and Rhone-Poulenc (Cranbury, NJ). Powders synthesized by proprietary wet-chemical techniques at these firms have been calcined and characterized by ANL. We have optimized the conditions for processing YBCO powders (Balachandran et al., 1992c) and have obtained highly promising results from Bi-based powders.

ANL is working with Ceracon Industries (Sacramento, CA) to develop and test electrical leads made from high-T_c superconductors. Ceracon uses its proprietary process to form the powders supplied by us into wires, cylinders, and other commercial shapes suitable for leads. We measure the ability of the leads to carry current at various temperatures and in the presence of various magnetic fields (Raman et al., 1992). Work on BSCCO materials is in progress.

The ANL patented low-pressure calcination technique (Balachandran et al., 1992b) is being used by Superconductive Components Inc. (Columbus, OH) to produce commercial quantities of high-grade YBCO and BSCCO powders.

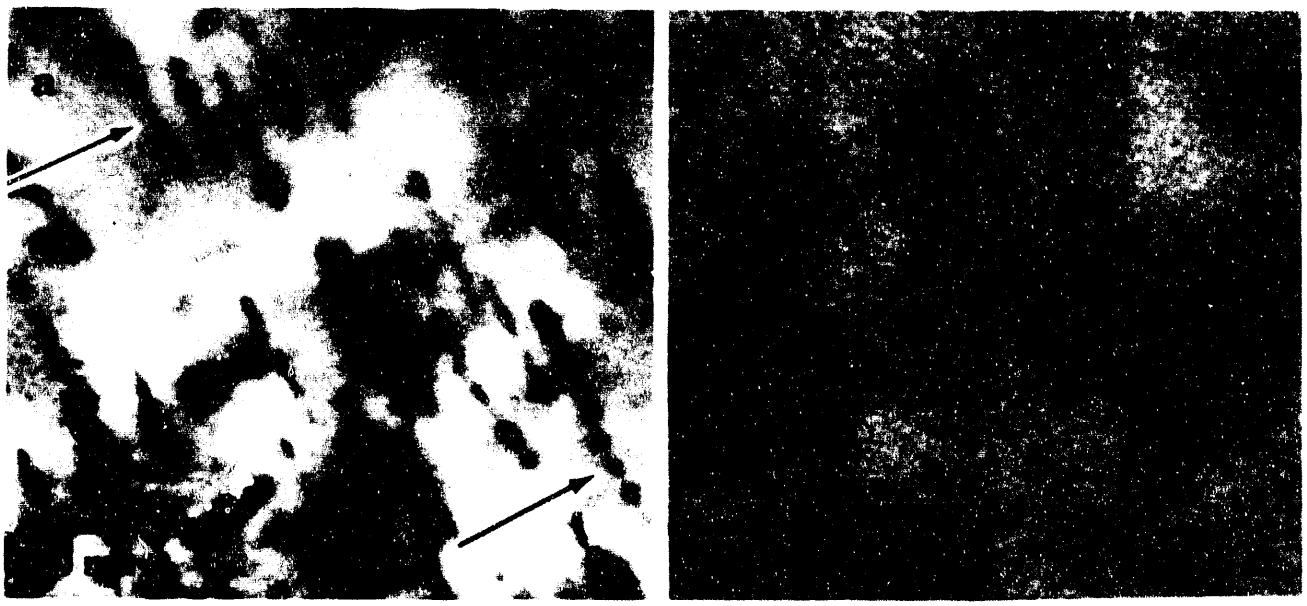

Fig. 22. TEM images of track morphology for (a) 580-MeV Sn and (b) 1.1-GeV Au irradiation of YBCO single crystals

We have collaborated with Lawrence Livermore National Laboratory to study the feasibility of shock consolidation to introduce flux-pinning defects into ceramic superconductors. YBCO was nearly saturated with dislocations ($\approx 10^{12}$ cm/cm^3) when shocked to 167 Kbar. T_c was unaffected. Bulk samples of crystallographically aligned BSCCO 2212 were fabricated by shock consolidation of tapped powders and the magnetic J_c was enhanced by a factor of 2–6 over that for statically pressed and sintered pellets.

University collaborations include work with Prof. N. G. Eror of the University of Pittsburgh on powder synthesis by freeze drying; high-resolution electron microscopy with Prof. V. Dravid of Northwestern University; work with Prof. Lynn Johnson of Northwestern University in the area of melt processing with microwave energy; collaboration with Prof. Jennifer Lewis of the University of Illinois at Urbana-Champaign focused on use of a magnetic field to align YBCO grains in the green state; texture analysis work on bulk YBCO and BSCCO with Prof. John Kallend of the Illinois Institute of Technology; creep testing of superconductors with Prof. Arturo Dominguez-Rodriguez of the University of Seville and Case Western Reserve University; and wire and tape forming by hot rolling of pure and Li-doped 2212, with Prof. Justin Schwartz of the University of Illinois at Urbana-Champaign.

The agreement between MagneTek (Los Angeles) and ANL to develop and build motor-winding prototypes has continued. Highly textured 2212 has been grown on MgO substrates. Microstructural analysis revealed that long crystallites were aligned along the solidification path. T_c values of 80 K were measured for many of these specimens. J_c values at 4.2 K were greater than 7500 A/cm^2 and were limited by contact resistance, not by the performance of the thick films (Risch et al., 1992). We are focusing on increasing T_c.

Levitation-melting work with Intersonics (Northbrook, IL) has progressed. A hybrid melter equippedd with a CO_2 laser has been used in two sets of experiments. In the first set, YBCO spheres were melted at various temperatures and cooled slowly to examine the

uniformity of the melt. In the second set, the spheres were splat-quenched to determine the phases present. Results indicate that, for melting above 1400°C, gross segregation occurs upon cooling. Quenching indicated that segregation in the melt was present on a scale of ≈10 μm. The phases were Y_2O_3 and a Ba/Cu-rich liquid. Future work will focus on making larger quantities of melt-quenched materials with high intragranular J_c.

We have continued to work with the Naval Surface Warfare Center (NSWC) on conductor development that is based on powder-in-tube processing. BSCCO powders made at ANL were packed in Ag tubes at NSWC and formed into wires. These samples were sintered at ANL under varying conditions of temperature and oxygen pressure and exhibited J_c values of ≈25,000 A/cm^2 at 4.2 K in a self-field. The sintered wires have been rolled into tapes at NSWC, and further heat treatments are being examined.

The collaborative program between ANL and Newport News Shipbuilding (NNS) is a multiyear/multiphase program that started in 1990. Funding has been obtained from NNS and the Office of Naval Research, in addition to that from the U.S. Department of Energy. The main objective of the project has been to demonstrate the feasibility of magnetohydrodynamic (MHD) seawater propulsion with high-T_c superconducting magnets. This has been accomplished by the development of computer models of thruster components, and by performing experiments to validate the adequacy of the models. A parametric study performed with the developed code during Phase I of the project has identified and confirmed the need for high-strength magnetic fields (10–20 T) to achieve attractive MHD thruster efficiencies (Fig. 23). The focus of the second phase has been to validate experimentally the thruster performance code and identify through testing any phenomena that might have an impact on the attractiveness of this propulsion system for shipboard applications.

Phase II of the MHD propulsion project consisted of three main tasks. Task 1 involved the design, construction, and assembly of a seawater MHD loop at an existing ANL facility. The test loop consists of a 2-T conventional electromagnet, a test section of the thruster, gas separator, a loop pump, piping and related fittings, and instrumentation. With the exception of the electrodes, the test section is fabricated entirely of optically clear polycarbonate to enable direct visual observation of electrolytically generated gaseous bubbles at the electrodes.

In Task 2, the loop was used to perform experiments at velocity and electric-current-density operating conditions characteristic of full-size marine vehicles. The facility is designed to provide a bubble generation rate comparable to projected operating conditions. Currents and voltages were measured at each electrode segment. Other measurements included the pressure distribution along the thruster, flow rate, electrical conductivity, and high-speed video camera measurements of bubble characteristics.

Task 3 included performing pre- and posttest analyses of the experiment. The pretest analysis was used to establish the baseline for the performance of the thruster and the test loop, and to provide guidance in establishing the test matrix by using the MHD thruster code developed during Phase I of the project. The results of the simulation test were compared with the predictions of the developed models, thus establishing confidence in the computer codes.

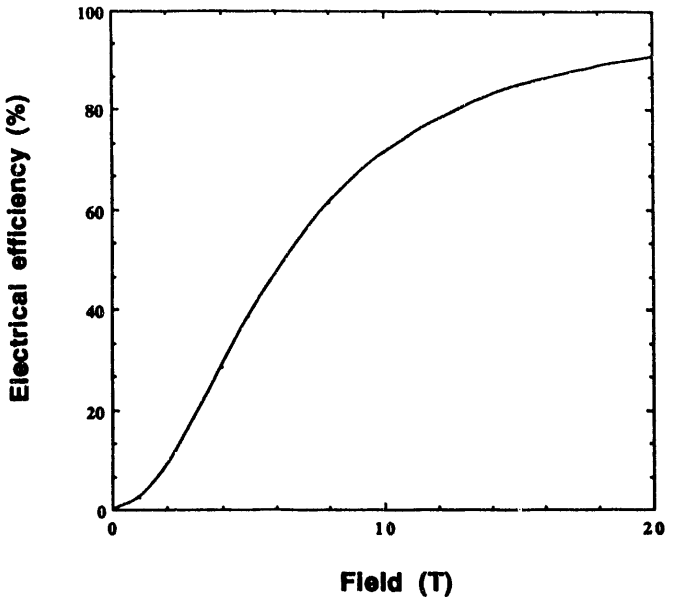

Fig. 23.
MHD thruster efficiency

Measurements were obtained for two different working fluids (an aqueous solution of NaCl and "Instant Ocean"), two fluid conductivities, and with horizontal and vertical magnetic fields to ascertain the effect of buoyancy on bubble characteristics. The test matrix included close to 500 individual data scans for different operating conditions. The thruster was modeled with a one-dimensional hydrodynamic model coupled to a two-dimensional electrical model. The thruster model included the major loss mechanisms that affect the performance of MHD thrusters. Among these are joule dissipation losses, frictional losses, electrical end losses, and electrode surface potential losses. The good agreement found between measured and predicted parameters served to validate the developed thruster code. Furthermore, the results indicate that production of hydrogen bubbles at the cathode does not appear to have an impact on propulsion performance for current densities relevant to full-size thrusters. Also, it was demonstrated that the thruster performance is independent of the orientation of the magnetic field relative to gravity. In general, the results of the tests and their comparison with predictions indicate that the phenomena affecting the performance of MHD seawater thrusters are well-understood and are adequately quantified with the developed computer codes (Doss and Geyer, 1992; Picologlou et al., 1992a, 1992b).

The best J_c values for bulk samples have been obtained in samples containing well-aligned microstructures. In a newly initiated collaboration with BASF (Asheville, NC), we are attempting to produce YBCO fibers with well-aligned grains without resorting to melt-processing. In this approach, ANL produces YBCO grains with plate-like morphology that are aligned at BASF by a proprietary fiber-spinning process. The green, aligned samples are then heat treated at ANL under reduced O_2 pressure to remove the organics without decomposing the YBCO. Work is in progress.

The collaboration with SuperconIX (St. Paul, MN) has continued. We have recently evaluated by SEM and XRD the microstructures of several 2212 thick films and have measured T_c and J_c. These films are being developed under a NASA contract for use in small-scale magnets.

We have begun a collaboration with Ames Laboratory to examine phase equilibria of PBSCCO 2223. Ames has made extensive use of high-temperature X-ray diffractometry to perform similar studies on the 2212 BSCCO compound (Polonka et al., 1991). Our initial focus is on the reaction kinetics of formation of 2223 from 2212. The first set of experiments has confirmed the importance of a liquid phase to the reaction.

References

V. Ambegaokar and B. I. Halperin, Phys. Rev. Lett. **22**, 1364 (1969).

K. Aota, H. Hattori, T. Hatano, K. Nakamura, and K. Ogawa, Jpn. J. Appl. Phys. **28**, L2196 (1989).

U. Balachandran, D. Shi, D. I. dos Santos, S. W. Graham, M. A. Patel, B. Tani, K. Vandervoort, H. Claus, and R. B. Poeppel, Physica C **156**, 649 (1988).

U. Balachandran, S. L. Morissette, R. A. Russell, S. E. Dorris, and R. B. Poeppel, in "High Temperature Superconducting Compounds III," eds. S. H. Whang, A. DasGupta, and E. W. Collings (The Metallurgical Society, Warrendale, PA, 1991), p. 273.

U. Balachandran, S. E. Dorris, M. T. Lanagan, and R. B. Poeppel, in "International Workshop on Superconductivity" (ISTEC, Tokyo, 1992a), p. 374.

U. Balachandran, R. B. Poeppel, J. E. Emerson, and S. A. Johnson, U.S. Patent 5,086,034, Feb. 4, 1992b.

U. Balachandran, J. M. Tourre, and J. W. Golowski, Mater. Res. Soc. Symp. Proc. **249**, 121 (1992c).

C. H. Bamford and C. F. H. Tipper, "Reactions in the Solid State" (Elsevier Scientific Publishing, New York, 1969).

A. C. Biondo, J. S. Kallend, A. J. Schultz, and K. C. Goretta, in "2nd World Congress on Superconductivity," ed. C. G. Burnham (World Scientific, Singapore, 1992), p. 361.

I. Bloom, J. R. Frommelt, M. C. Hash, M. T. Lanagan, C.-T. Wu, and K. C. Goretta, Mater. Res. Bull. **26**, 1269 (1991).

R. Bormann and J. Nölting, Appl. Phys. Lett. **54**, 2148 (1989).

Y. S. Cha, J. R. Hull, and U. S. Choi, IEEE Trans. Supercond., in press (1992).

N. Chen, D. Shi, and K. C. Goretta, J. Appl. Phys. **66**, 2485 (1989).

N. Chen, S. J. Rothman, J. L. Routbort, and K. C. Goretta, J. Mater. Res. **7**, 2308 (1992a).

N. Chen, J. L. Routbort, K. C. Goretta, J. P. Singh, and R. B. Poeppel, in "International Workshop on Superconductivity" (ISTEC, Tokyo, 1992b), p. 130.

C.-Y. Chu, J. L. Routbort, N. Chen, A. C. Biondo, D. S. Kupperman, and K. C. Goretta, Supercond. Sci. Technol. **5**, 306 (1992).

L. Civale, A. D. Marwick, M. W. McElfresh, T. K. Worthington, A. P. Malozemoff, F. H. Holtzberg, J. R. Thompson, and M. A. Kirk, Phys. Rev. Lett. **65**, 1164 (1990).

L. Civale, A. D. Marwick, M. W. McElfresh, T. K. Worthington, A. P. Malozemoff, F. H. Holtzberg, C. Field, J. R. Thompson, D. K. Christen, and M. A. Kirk, in "Proc. XII Winter Meeting on Low-Temperature Physics, Cuernavaca, Mexico" (World Scientific, Singapore, 1991).

S. E. Dorris, J. T. Dusek, M. T. Lanagan, J. J. Picciolo, J. P. Singh, J. E. Creech, and R. B. Poeppel, Am. Ceram. Soc. Bull. **70**, 722 (1991).

E. Doss and H. K. Geyer, in Proc. 27th Intersociety Energy Conversion Engineering Conf. (IECEC, San Diego, 1992), Vol. 3, p. 299.

K. C. Goretta, J. G. Chen, N. Chen, M. C. Hash, and Donglu Shi, Mater. Res. Bull. **25**, 791 (1990a).

K. C. Goretta, J. L. Routbort, A. C. Biondo, Y. Gao, A. R. de Arellano-López, and A. Dominguez-Rodriguez, J. Mater. Res. **5**, 2766 (1990b).

K. C. Goretta, M. L. Kullberg, D. Bär, G. A. Risch, and J. L. Routbort, Supercond. Sci. Technol. **4**, 544 (1991).

K. C. Goretta, N. Chen, M. T. Lanagan, S. E. Dorris, J. Hu, C.-T. Wu, and R. B. Poeppel, Supercond. Sci. Technol. **5**, 534 (1992a).

K. C. Goretta and D. Shi, Appl. Phys. Commun. **11**, 317 (1992).

K. C. Goretta, C.-T. Wu, M. T. Lanagan, M. A. Boling, D. Shi, D. J. Miller, N. Chen, W. G. Hanewald, S. Sengupta, Z. Wang, and R. B. Poeppel, Mater. Res. Soc. Symp. Proc. **275**, 813 (1992b).

K. C. Goretta, D. J. Miller, R. B. Poeppel, A. S. Nash, Mater. Res. Soc. Symp. Proc. **251**, 325 (1992c).

G. S. Grader, E. M. Gyorgy, P. K. Gallagher, H. M. O'Bryan, D. W. Johnson Jr., S. Shushine, S. M. Zahurak, S. Jin, and R. C. Sherwood, Phys. Rev. **B38**, 757 (1988).

P. Haldar, J. G. Hoehn, J. A. Rice, L. R. Motowidlo, U. Balachandran, C. A. Youngdahl, J. E. Tkaczyk, and P. J. Bednarczyk, IEEE Trans. Supercond., in press (1992).

T. Hatano, K. Aota, S. Ikeda, K. Nakamura, and K. Ogawa, Jpn. J. Appl. Phys. **27**, L2055 (1988).

J. D. Hettinger, D. H. Kim, D. J. Miller, J. G. Hu, K. E. Gray, J. E. Sharping, K. Daly, C. Pettiette-Hall, J. E. Tkaczyk, and J. DeLuca, IEEE Trans. Supercond., in press (1992).

S. Hirano, T. Hayashi, and M. Miura, J. Am. Ceram. Soc. **73**, 885 (1990).

B. Hong, J. Hahn, and T. O. Mason, J. Am. Ceram. Soc. **73**, 1965 (1990).

S. F. Hulbert, J. Brit. Ceram. Soc. **6**, 11 (1969).

J. R. Hull, Y. S. Cha, and U. S. Choi, "Cryostabilization of High-Temperature Superconductors," Invention Disclosure ANL-IN-92-014, patent pending.

S. Jin and J. E. Graebner, Mater. Sci. Eng. **B7**, 243 (1991).

J. Joo, J. P. Singh, R. B. Poeppel, A. K. Gangopadhyay, and T. O. Mason, J. Appl. Phys. **71**, 2351 (1992).

D. Y. Kaufman, M. T. Lanagan, S. E. Dorris, J. T. Dawley, I. D. Bloom, M. C. Hash, N. Chen, M. R. DeGuire, and R. B. Poeppel, Appl. Supercond. **1**, 81 (1993).

D. H. Kim, K. E. Gray, R. T. Kampwirth, J. C. Smith, D. S. Richeson, T. J. Marks, J. H. Kang, J. Talvacchio, and M. Eddy, Physica C **177**, 431 (1991).

D. H. Kim, K. E. Gray, and J. D. Hettinger, unpublished information (1992).

M. Kirk, Mater. Res. Soc. Symp. Proc. **209**, 743 (1991).

D. S. Kupperman, J. P. Singh, J. Faber Jr., and R. L. Hitterman, J. Appl. Phys. **66**, 3396 (1989).

S. Koyama, U. Endo, and T. Kawai, Jpn. J. Appl. Phys. **27**, L1861 (1988).

T. B. Lindemer, C. R. Hubbard, and J. Brynestad, Physica C **167**, 312 (1990).

J. Luine, J. Bulman, J. Burch, K. Daly, A. Lee, C.Pettiette-Hall, S. Schwarzbek, and D. Miller, Appl. Phys. Lett. **61**, 1128 (1992).

J. S. Luo, N. Merchant, V. A. Maroni, E. Escorcia-Aparicio, D. M. Gruen, B. S. Tani, G. N. Riley Jr., and W. L. Carter, IEEE Trans. Supercond., in press (1992).

H. M. Meyer III, D. M. Hill, T. J. Wagener, J. H. Weaver, C. F. Gallo, and K. C. Goretta, J. Appl. Phys. **65**, 3130 (1989).

D. J. Miller, S. Sengupta, J. D. Hettinger, D. Shi, K. E. Gray, A. S. Nash, and K. C. Goretta, Appl. Phys. Lett. **61**, 2823 (1992).

T. A. Miller, J. E. Ostenson, Q. Li, L. A. Schwartzkopf, D. K. Finnemore, J. Righi, R. A. Gleixner, and D. Zeigler, Appl. Phys. Lett. **58**, 2159 (1991).

M. Murakami, M. Morita, and N. Koyama, Jpn. J. Appl. Phys. **28**, L1754 (1989).

S. Soo Oh and K. Osamura, Supercond. Sci. Technol. **4**, 239 (1991).

B. F. Picologlou, E. D. Doss, D. Black, and W. C. Sikes, in Proc. 27th Intersociety Energy Conversion Engineering Conf. (IECEC, San Diego, 1992a), Vol. 3, p 305.

B. F. Picologlou, E. D. Doss, H. K. Geyer, W. C. Sikes, and R. F. Ranellone, in "11th International Conference on MHD Electrical Power Generation," Beijing, China, October 12-16, in press (1992b).

R. B. Poeppel et al., "Practical Superconductor Development for Electrical Power Applications: Annual Report for FY 1990," Argonne National Laboratory Report ANL-90/47 (1990).

R. B. Poeppel et al., "Practical Superconductor Development for Electrical Power Applications: Annual Report for FY 1991," Argonne National Laboratory Report ANL-91/28 (1991).

R. B. Poeppel, K. C. Goretta, U. Balachandran, S. E. Dorris, M. T. Lanagan, J. J. Picciolo, C. A. Youngdahl, and D. I. dos Santos, Braz. J. Phys. **22**, 53 (1992).

R. B. Poeppel, U. Balachandran, S. E. Dorris, J. Joo, D. Y. Kaufman, M. T. Lanagan, B. C. Prorok, J. P. Singh, C.-T. Wu, and K. C. Goretta, Appl. Supercond. **1**, in press (1993).

J. Polonka, M. Xu, Q. Li, A. I. Goldman, and D. K. Finnemore, Appl. Phys. Lett. **59**, 3640 (1991).

R. V. Raman, S. V. Rele, U. Balachandran, and R. B. Poeppel, in "International Workshop on Superconductivity" (ISTEC, Tokyo, 1992) p. 364.

G. A. Risch, M. T. Lanagan, K. C. Goretta, and B. M. Moon, Mater. Lett. **12**, 291 (1991).

G. A. Risch, M. T. Lanagan, R. B. Poeppel, and M. R. DeGuire, Supercond. Sci. Technol. **5**, 542 (1992).

J. L. Routbort, K. C. Goretta, D. J. Miller, D. B. Kazelas, C. Clauss, and A. Dominguez-Rodriguez, J. Mater. Res. **7**, 2360 (1992).

S. Sengupta, D. Shi, Z. Wang, A. C. Biondo, U. Balachandran, and K. C. Goretta, Physica C **199**, 43 (1992).

M. Seido, J. Sato, T. Sasaoka, A. Nomoto, T. Umezawa, M. Okada, K. Aihara, and S. Matsuda, Appl. Supercond. **1**, in press (1993).

D. Shi, M. S. Boley, J. G. Chen, M. Xu, K. Vandervoort, Y. X. Liao, A. Zangvil, J. Akujieze, and C. Segre Appl. Phys. Lett. **55**, 699 (1989).

J. P. Singh, H. J. Leu, R. B. Poeppel, E. Van Voorhees, G. T. Goudey, K. Winsley, and D. Shi, J. Appl. Phys. **66**, 3154 (1989).

J. P. Singh, R. A. Guttschow, D. T. Dusek, and R. B. Poeppel, J. Mater. Res. **7**, 2324 (1992).

J. P. Singh, J. Joo, D. Singh, T. Warzynski, and R. B. Poeppel, J. Mater. Res., in press (1993).

J. R. Thompson, Y. R. Sun, H. R. Kerchner, B. C. Sales, B. C. Chakoumakos, A. D. Marwick, L. Civale, and J. O Thompson, Appl. Phys. Lett. **60**, 2306 (1992).

J. E. Tkaczyk, J. A. DuLuca, P. L. Karas, P. J. Bednarczyk, M. F. Garbauskas, R. H. Arendt, K. W. Lax, and J. S. Moodesa, Appl. Phys. Lett. **61**, 610 (1992).

J. Tsuchiya, H. Endo, N. Kijima, A. Sumiyama, M. Mizuno, and Y. Oguri, Jpn. J. Appl. Phys. **29**, L1918 (1989).

B. R. Weinberger, L. Lynds, and J. R. Hull, Supercond. Sci. Technol. **3**, 381 (1990).

B. R. Weinberger, L. Lynds, J. R. Hull, and U. Balachandran, Appl. Phys. Lett. **59**, 1132 (1991).

A. M Wolsky et al., Argonne National Laboratory Report ANL/CNSV-64 (1988).

C.-T. Wu, K. C. Goretta, D. Shi, and R. B. Poeppel, in "High Temperature Superconducting Compounds III," eds. S. H. Whang, A. DasGupta, and E. W. Collings (The Metallurgical Society, Warrendale, PA, 1991) p. 375.

C.-T. Wu, K. C. Goretta, and R. B. Poeppel, Appl. Supercond. **1**, 31 (1993).

J. L. Wu, J. T. Dederer, P. W. Eckels, S. K. Singh, J. R. Hull, R. Poeppel, C. A. Youngdahl, J. P. Singh, M. T. Lanagan, and U. Balachandran, IEEE Trans. Magn. **27**, 1861 (1991).

Y. Yamada, B. Obst, and R. Flukiger, Supercond. Sci. Technol. **4**, 165 (1991).

Distribution for ANL-92/38

Internal:

T. Askew
U. Balachandran
I. D. Bloom
S. Borys
M. B. Brodsky
N. Browning
Y. S. Cha
N. Chen
G. Crabtree
D. R. Diercks
S. E. Dorris
E. Doss
H. Drucker
B. Dunlap
J. T. Dusek
W. A. Ellingson
J. E. Emerson
F. Y. Fradin
R. Giese
K. C. Goretta
K. E. Gray
D. Gruen
M. Hanley
M. Hash
J. Hettinger
J. Hu
J. R. Hull
J. Jorgensen
R. T. Kampwirth
M. Kirk
D. S. Kupperman
S. Lake
M. T. Lanagan
C. A. Malefyt (2)
V. A. Maroni
R. L. McDaniel
D. J. Miller
S. Morissette
T. Mulcahy
R. C. Niemann
J. J. Picciolo
R. B. Poeppel (15)
A. C. Raptis
J. L. Routbort
W. J. Shack
T. P. Sheahen
J. P. Singh
C. E. Till
K. L. Uherka
A. Wagh
A Wantroba
R. W. Weeks
R. Wheeler
A. M. Wolsky
C. A. Youngdahl
ANL Patent Dept.
TIS Files

External:

DOE-OSTI, for distribution per UC-201 (12)
ANL Libraries
ANL-E
ANL-W

DOE Chicago Field Office:
Manager
F. Herbaty

U.S. Department of Energy, Washington:

Office of Advanced Utility Concepts, Conservation and Renewable Energy:
J. Daley
R. Eaton III
M. Gunn
Basic Energy Sciences-Materials Science, Energy Research:
I. L. Thomas

Materials and Components Technology Division Review Committee:
H. K. Birnbaum, University of Illinois at Urbana-Champaign, Urbana
R. C. Buchanan, University of Cincinnati, Cincinnati, OH
M. S. Dresselhaus, Massachusetts Institute of Technology, Cambridge, MA
B. G. Jones, University of Illinois at Urbana-Champaign, Urbana

C.-Y. Li, Cornell University, Ithaca, NY
S.-N. Liu, Electric Power Research Institute, Palo Alto, CA
R. E. Smith, Engineering Applied Sciences, Inc., Trafford, PA

Other - Industry - University
J. Badin, Energetics, Inc.
T. Bickel, Sandia National Laboratories
R. W. Boom, University of Wisconsin - Madison
J. Bray, General Electric Company
R. Cass, HiTc Superconco, Inc.
D. L. Chung, State University of New York - Buffalo
J. Clem, Ames Laboratory
R. Colwell, MagneTek Universal Electric
B. Currie, Pacific Northwest Laboratory
S. Danyluk, University of Illinois at Chicago
M. Daugherty, Superconductivity, Inc.
M. DeGuire, Case Western Reserve University
L. P. de Rochemont, Radiation Monitoring Devices, Inc.
D. Divecha, Naval Surface Warfare Center
B. Dorothy, DuPont
M. Eddy, Superconductor Technologies, Inc.
N. Eror, University of Pittsburgh
D. K. Finnemore, Ames Laboratory
M. Fluss, Lawrence Livermore National Laboratory
S. Foner, Francis Bitter National Magnet Lab., Massachusetts Institute of Technology
J. R. Gaines, Superconductive Components, Inc.
C. Gallo, Superconix
T. Grudkowski, United Technologies Research Center
D. Gubser, Naval Research Laboratory
P. Haldar, Intermagnetics General Corp.
S. D. Harkness, Westinghouse
R. A. Hawsey, Oak Ridge National Laboratory
H. Herro, Nalco Chemical Company
J. Hodge, Illinois Superconductor Corp.
D. L. Johnson, Northwestern University
H. Jordan, Reliance Electric
J. B. Ketterson, Northwestern University
J. L. Kirtley, Jr., Massachusetts Institute of Technology
M. Klein, University of Illinois at Urbana-Champaign
D. K. Kroeger, Oak Ridge National Laboratory
H. Kroger, Microelectronics and Computer Technology Corporation
D. C. Larbalestier, University of Wisconsin - Madison
A. Lauder, DuPont
E. Leung, General Dynamics
M. Levy, University of Wisconsin - Milwaukee
J. Lewis, University of Illinois at Urbana-Champaign
D. H. Liebenberg, Office of Naval Research
R. Loehman, Sandia National Laboratories
J. Loncoski, Virginia Power
H. Madler, J. C. Petlau, Inc.
D. Madura, General Dynamics
A. Malozemoff, American Superconductor Corp.

M. Marinelli, University of Genova, Italy
C. Martin, SSC, Inc.
A. Marwick, IBM
T. Mason, Northwestern University
R. Mathisen, Foster-Miller, Inc.
B. McConnell, National Renewable Energy Laboratory
P. J. McGinn, University of Notre Dame
F. C. Moon, Cornell University
L. Motowidlo, IGC Advanced Superconductors, Inc.
D. N. Palmer, ABB, Inc.
C. A. Parker, Allied Signal, Inc.
D. Peterson, Los Alamos National Laboratory
N. Phillips, Lawrence Berkeley Laboratory
R. Raman, Ceracon
R. F. Ranellone, Newport News Shipbuilding
R. A. Roehl, Commonwealth Edison Company
C. H. Rosner, Intermagnetics General Corp.
J. Rowell, Conductus
D. K. Sharma, Electric Power Research Institute
S. Sinha, University of Illinois at Chicago
G. Smith, SSC, Inc.
O. Smith, Illinois Superconductor Corp.
D. M. Smyth, Lehigh University
M. Suenaga, Brookhaven National Laboratory
R. Troendly, Shaped Wire, Inc.
P. T. Tsivitse, Reliance Electric
O. Tuominen, BASF Corp.
R. Weber, Intersonics Corp.
B. Weinberger, United Technologies Research Center
D. O. Welch, Brookhaven National Laboratory
R. E. Williams, Ocean and Atmospheric Science, Inc.
J. Wu, Westinghouse Electric Corporation, Science and Technology Center
K. Youngdahl, Boeing Corporation
G. J. Yurek, American Superconductor Corporation
C. Zahopoulos, Northeastern University

END

DATE FILMED

3/22/93